CR-159818
PWA-5550-37

NASA

MODEL AERODYNAMIC TEST RESULTS FOR TWO VARIABLE CYCLE ENGINE COANNULAR EXHAUST SYSTEMS AT SIMULATED TAKEOFF AND CRUISE CONDITIONS

By D.P. Nelson

Commercial Products Division
Pratt & Whitney Aircraft Group
United Technologies Corporation

Prepared for
NATIONAL AERONAUTICS AND SPACE ADMINISTRATION
Lewis Research Center
Under
Contract NAS3-20061

TABLE OF CONTENTS

LIST OF TABLES

LIST OF ILLUSTRATIONS

LIST OF ILLUSTRATIONS (Continued)

LIST OF ILLUSTRATIONS (Continued)

LIST OF ILLUSTRATIONS (Continued)

LIST OF ILLUSTRATIONS (Continued)

SECTION 1.0

SUMMARY

This program is a continuation of the experimental and design study programs conducted by Pratt & Whitney Aircraft for advanced propulsion systems intended for a second-generation supersonic cruise aircraft. The program was directed towards evaluating the aerodynamic performance of two coannular exhaust systems at simulated takeoff and cruise conditions.

Wind tunnel performance tests were conducted using scale models of two variable-geometry coannular ejector nozzle configurations. The selection of these designs was based on low jet noise and the potential for good supersonic cruise performance. The main difference in the two designs is that one uses a short flap nozzle mechanism for fan stream control with an isentropic contoured splitter, while the other employs an iris fan nozzle with a conical flow splitter. Both designs simulate a translating primary plug for primary flow control and an actuated auxiliary inlet ejector. Three models of each exhaust system, approximately one-tenth scale (21.6 cm (8.5 in) diameter) were fabricated and tested in the NASA Lewis 8 by 6-Foot Supersonic Wind Tunnel. The models simulated takeoff, subsonic cruise, and supersonic cruise configurations of the full scale designs.

Over 200 data points were acquired at test Mach numbers of 0, 0.36, 0.9, and 2.0 for a wide range of nozzle operating conditions. The subsonic cruise iris configuration was also tested over an expanded range of subsonic Mach numbers. Aerodynamic test variables included fan nozzle pressure ratio and fan to primary pressure split commensurate with engine operation at each flight regime. In addition, the supersonic cruise configurations were tested with ejector secondary flow rates of zero, 2, and 4 percent relative to the combined flows of the fan and primary streams. Model geometric variables were ejector inlet area and the clamshell reverser position for the takeoff and subsonic cruise configurations. Fan and primary nozzle areas were varied to match desired engine operating conditions.

At a simulated supersonic cruise operating condition both configurations demonstrated good performance, comparable to levels assumed in earlier Advanced Supersonic Transport (AST) propulsion studies. At zero secondary flow, the gross thrust coefficients of the iris and short flap configurations were 0.980 and 0.984, respectively. Addition of secondary flow increased the iris nozzle thrust performance as much as 4.1 percent, while performance of the short flap configuration increased as much as 3.5 percent. Variation of fan to primary pressure split had no effect on nozzle gross thrust coefficient.

At the subsonic cruise operating condition ($M_0 = 0.9$), the performance of both configurations was deficient relative to the Advanced Supersonic Transport study level of 0.94. The maximum thrust coefficient was 0.880 for the iris configuration and 0.865 for the short flap configuration. Variations in ejector inlet area and the clamshell reverser position produced little effect on nozzle performance. Exploratory tests of the subsonic cruise configurations showed that inadequate ventilation of the ejector shroud resulted in excessive ejector inlet boattail drag.

Performance of the iris takeoff configuration approached the Advanced Supersonic Transport study level of 0.984, demonstrating a thrust coefficient of 0.980 at static conditions and 0.960 at climbout (M_0 = 0.3). The short flap configuration, however, was deficient by 4 and 6 percent, respectively, at these conditions. Additional tests of the takeoff configurations showed that the unsatisfactory performance of the short flap configuration resulted from an interaction of the fan nozzle flow with the ejector inlet flap. The tests also showed that the jet flow of the iris configuration impinged on the reverser clamshell.

SECTION 2.0

INTRODUCTION

2.1 BACKGROUND

For the past six years, Pratt & Whitney Aircraft has participated in a series of NASA sponsored programs aimed at establishing a technology base for a second-generation advanced supersonic commercial transport. A result of this work (Reference 1) has been the identification of the Variable Stream Control Engine as a very attractive engine configuration in terms of system performance and potential for low noise. Also, these studies indicated that a low jet noise, high performance coannular nozzle with variable geometry capability is a critical component in the Variable Stream Control Engine propulsion system.

Under NASA direction, a separate ongoing Coannular Nozzle Technology Program has focused on the aerodynamic/acoustic characteristics of the coannular exhaust system operating in the takeoff flight regime. Results of these programs (References 2 and 3) have demonstrated the ability of a coannular nozzle system with an inverted velocity profile to exhibit jet noise reduction benefits for both static and simulated takeoff flight conditions. A further result was the development of an aerodynamic/acoustic prediction procedure for inverted velocity profile coannular nozzles (Reference 4). This procedure is capable of predicting jet noise as a function of nozzle geometry, operating condition, and flight effects in the low speed flight regime.

Current effort in the program, as presented in this report, extends the demonstration of coannular exhaust system performance to key supersonic and subsonic flight conditions. Problem areas with current Advanced Supersonic Transport exhaust system designs and available performance procedures for evaluating the designs are defined.

2.2 PROGRAM DESCRIPTION

Two concepts of a variable-geometry coannular ejector nozzle were identified as promising configurations for the Variable Stream Control Engine exhaust system. These included a baseline and an alternate configuration. The selection of both designs was based on the potential for low jet noise at takeoff and good supersonic cruise thrust performance. The baseline configuration consisted of a variable-area short flap fan nozzle with a contoured flow splitter. The alternate configuration employed a variable-area iris flap fan nozzle with a conical flow splitter. The iris flap was chosen for potentially better subsonic performance. Common to both configurations was a translating plug in the primary stream and an actuated inlet ejector shroud with a clamshell reverser. Three configurations, approximately one-tenth scale, of each design were tested in the NASA Lewis 8 by 6-Foot Supersonic Wind Tunnel. The models simulated takeoff, subsonic cruise, and supersonic cruise configurations of full scale exhaust systems.

Over 200 data points were acquired for the six models at wind tunnel Mach numbers of 0, 0.36, 0.9, and 2.0 for a wide range of nozzle operating conditions. The subsonic cruise iris configuration was also tested at other subsonic Mach numbers. Fan and primary nozzle areas were varied to satisfy Variable Stream Control Engine operating requirements, while fan and primary pressure ratios were varied along with ejector inlet area and clamshell position. In addition, the supersonic configurations were tested with 0, 2, and 4 percent secondary ejector flow relative to the total flow of the fan and primary nozzle streams. Tests were also conducted with a modified Supersonic Tunnel Association nozzle to verify the facility thrust and flow measuring systems. The results of these tests are contained in Appendix A.

Nozzle charging station pressure, temperature, and weight flow were measured for each stream along with nozzle generated thrust. Data were analyzed in terms of nozzle thrust and discharge coefficients. Model surface static pressures were also measured. The results of the test program are presented in this report. Detailed data are presented in the companion Comprehensive Data Report (Reference 5).

The author wishes to acknowledge Douglas Harrington of the NASA Lewis Research Center for his assistance in conducting the test program and contributions to this report.

SECTION 3.0

FACILITY AND TEST EQUIPMENT

3.1 TEST FACILITY

The test program was conducted in the NASA Lewis 8 by 6 Foot Supersonic Wind Tunnel (Reference 6). Test nozzles were attached to a 21.59 cm (8.5 in) diameter cylindrical model supported in the test section by a perpendicular strut connected to the tunnel ceiling, as shown in Figures 3.1-1 and 3.1-2. Air was supplied to the model through long, flexible tubes running down the strut into coannular air passages that carried the air aft to the test model. The air supply tubes were fixed to the tunnel ceiling at the top, which was nonmetric (forces here were not transmitted to the load cell), and to the coannular air passages at the bottom. Air flow from the tubes entered the coannular passages normal to the model centerline and thus eliminated any entering axial momentum force on the load cell. Static pressure instrumentation was located on the internal upstream facing surfaces of the metric hardware to account for tare forces that result when internal static pressures were different from ambient.

Nozzle thrust was measured with a load cell mounted in the forward portion of the model. The air passages, supported by bearings at the front and rear, made contact with the load cell and were metric, i.e., axial forces acting on the model support coannular piping were measured by the load cell. The load cell was calibrated by applying a known axial force along the centerline of the model. This force was generated by using a hydraulic cylinder connected to the model with the shaft of the cylinder pushing along the axis of the nozzle. The correlation of the known applied force and the electrical output of the load cell provided the desired calibration which was from 0 to 8896 Newtons (2000 lbs.), the maximum allowable balance load.

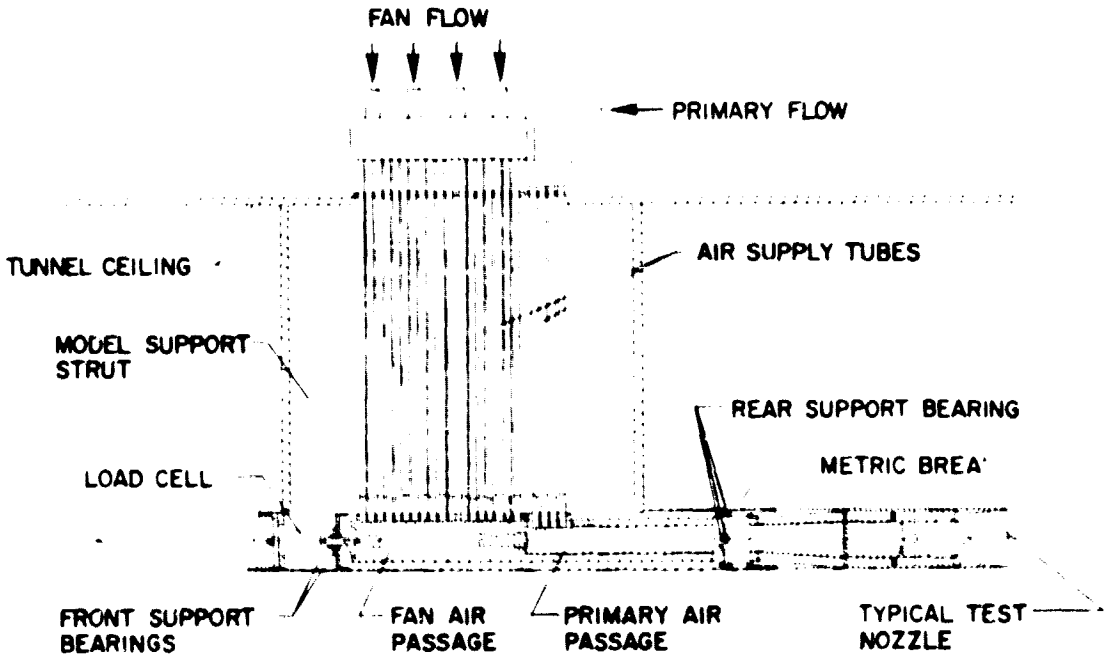

Figure 3.1-1 Diagram of Model Installed in Wind Tunnel

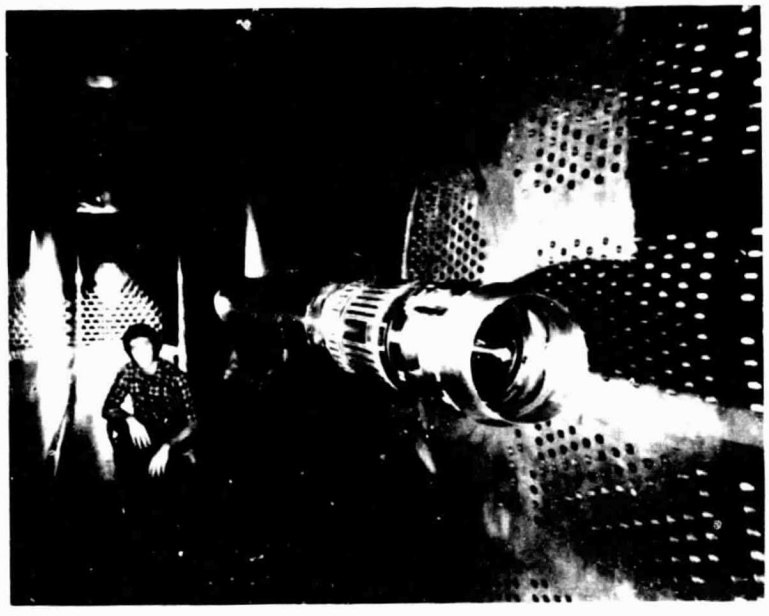

Figure 3.1-2 *Model Installed in NASA Lewis 8-by-6 Foot Supersonic Wind Tunnel*

A schematic of the air supply system is shown in Figure 3.1-3. The air source was a compressor that provided a continuous supply at 310 N/cm^2 (450 psig). After passing through a gas-fired heat exchanger, the air flowed through a system of control valves and flowmeter, and finally into the model strut. The heater was used only at supersonic cruise (i.e., a free stream Mach number of 1.96) where the tunnel total air temperature reaches 93°C (200°F). To minimize temperature gradients in the model, air was heated to 66°C (150°F). At all other test Mach numbers, the model air was not heated.

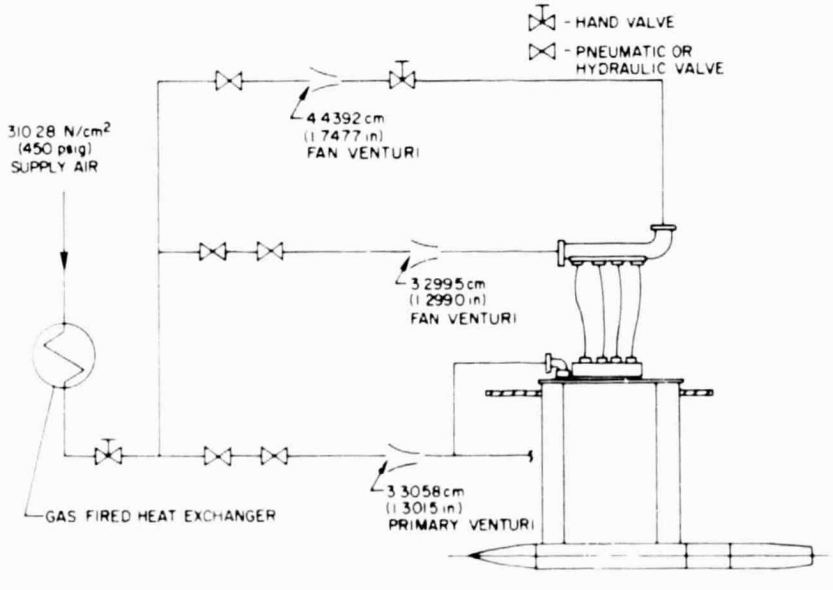

Figure 3.1-3 *Model Air Supply System*

Primary nozzle air was metered with a choked venturi which had a 3.3058 cm (1.3015 in) throat diameter. Fan nozzle air supply was metered through either a 4.4392 cm (1.7477 in) or 3.2995 cm (1.2990 in) diameter choked venturi, depending on the flow rate required.

Tests were conducted with a modified Supersonic Tunnel Association nozzle to verify the facility thrust and flow measuring systems. The results of these tests are described in Appendix A.

3.2 EXHAUST NOZZLE SYSTEM REQUIREMENTS

The exhaust system requirements for a duct burning turbofan propulsion system were established on the basis of a combination of engine characteristics and mission and acoustic considerations. The operating conditions (nozzle pressure ratios and areas) of the Variable Stream Control Engine 502B (Reference 1), are tabulated in Table 3.2-I for the key flight conditions tested. As shown, independent fan and primary nozzle area control is required. The largest area variation occurs in the fan stream where a 3 to 1 area change is needed for engine operation. Nozzle performance/range trade factors for a supersonic mission indicate that supersonic cruise is the critical design point. The mission analysis established that one percent in supersonic cruise nozzle performance is worth 270 km (168 mi) range for an overall 7364 km (4700 mi) mission. Similarly, one percent in subsonic nozzle performance yields only 34 km (21 mi) range increments. The nozzle performance levels assumed for the Advanced Supersonic Transport propulsion studies are shown in Table 3.2-II. Acoustics becomes important because of takeoff jet noise requirements. Previous acoustic tests indicate that a coannular nozzle configured with a high radius ratio fan nozzle annulus and inverted velocity profile allows rapid mixing of the high velocity fan stream, reducing overall jet noise. Finally, the exhaust system must be capable of thrust reversal.

TABLE 3.2-I

VSCE-502B OPERATING CONDITIONS AT KEY FLIGHT CONDITIONS

(409 kg/sec (900 lb/sec) flow size), Reference 1

Flight Condition	P_{tf}/P_o	Fan Stream Throat Area, A_{18} $m^2(ft^2)$	P_{tf}/P_{tp}	Primary Stream Throat Area, A_8 m^2 (ft^2)
Takeoff - Low Noise	2.49	1.106(11.91)	1.46	0.749(8.06)
Takeoff - Design	3.14	0.766(8.25)	1.70	0.749(8.06)
Subsonic Cruise	5.26	0.367(3.95)	1.97	0.792(8.53)
Supersonic Cruise	27.5	0.511(5.50)	2.32	0.797(8.58)

TABLE 3.2-II

NOZZLE PERFORMANCE ASSUMED FOR

ADVANCED SUPERSONIC TRANSPORT STUDIES

Flight Condition	Mach Number	Gross Thrust Coefficient (C_{fg})*
Takeoff		
Static	0.0	0.984
Climb Out	0.3	0.983
Subsonic Cruise	0.9	0.940
Supersonic Cruise	2.3	0.982

*No Secondary flow

3.2.1 Exhaust Nozzle System Design

A nozzle design to meet the requirements outlined in Section 3.2 was defined in a preliminary nozzle design study (Reference 1). The features of this design are incorporated in an early engine design in Figure 3.2-1 and include: a variable-area convergent-divergent (C-D) primary nozzle incorporated in the fan-primary gas path flow splitter, a variable-area iris flap fan nozzle, an actuated ejector inlet with variable-area trailing edge flaps, and a clamshell reverser. Refinements of this design formed the basis for the test configurations.

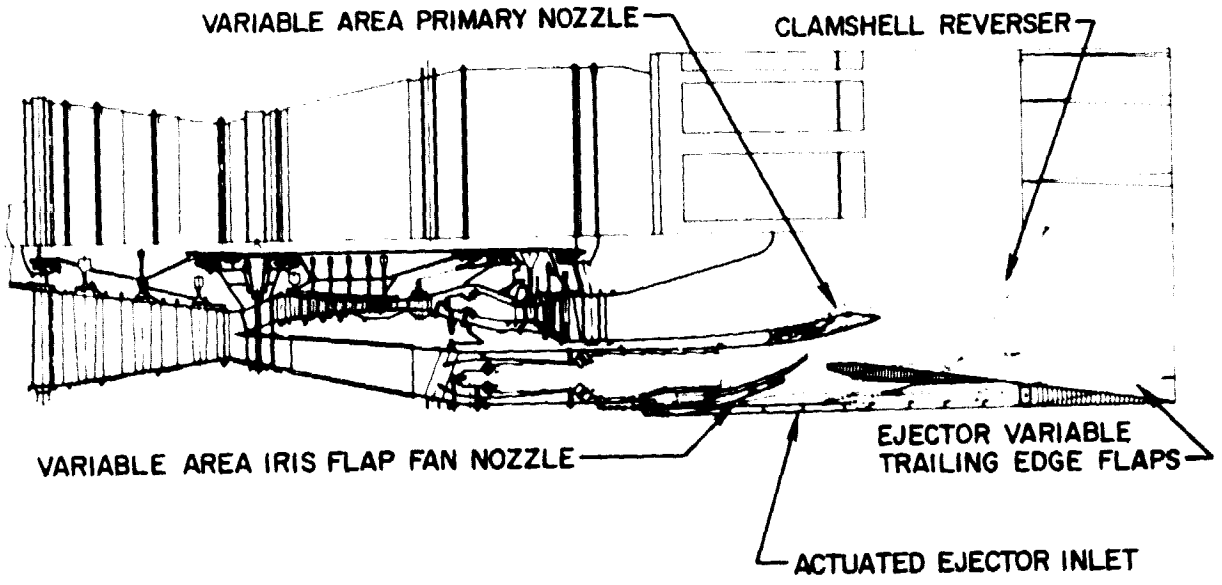

Figure 3.2-1 Variable Stream Control Engine (VSCE-502B)

A flow analysis of the configuration in the supersonic cruise mode revealed a potential internal performance loss due to the splitter design. The analysis indicated that the impingement angle of the fan and primary flows at the splitter trailing edge would create a strong shock loss. However, predictions of overall internal performance were not possible because of difficulties encountered in the analysis of the complete flow field. The exhaust system was redesigned to eliminate this shock loss, as shown in Figure 3.2-2, with an isentropic contoured splitter, so that the merging fan and primary flows would exit nearly parallel. The design reflects the minimum overall length required for optimum thrust-minus-drag at the critical supersonic cruise operating condition. The design was not compromised with the increased length, i.e., friction drag and weight, required to optimize performance at off-design mission conditions. As a result of geometry limitations, this splitter modification required the addition of a translating centerbody plug to provide primary nozzle area control. To avoid primary overexpansion losses in the takeoff mode, the center portion of the plug translates aft to form the nozzle throat at the splitter trailing edge. The axial translation inherent with the iris flap mechanism (Figure 3.2-3), in conjunction with the contoured splitter, would result in large off-design losses because of uncontrolled overexpansion and flow turning. Therefore, the iris flap was replaced with a hinged short flap nozzle that rotated in a radial plane to provide fan area variation. This redesigned exhaust system provided the flow path lines for the short flap nozzle test configurations.

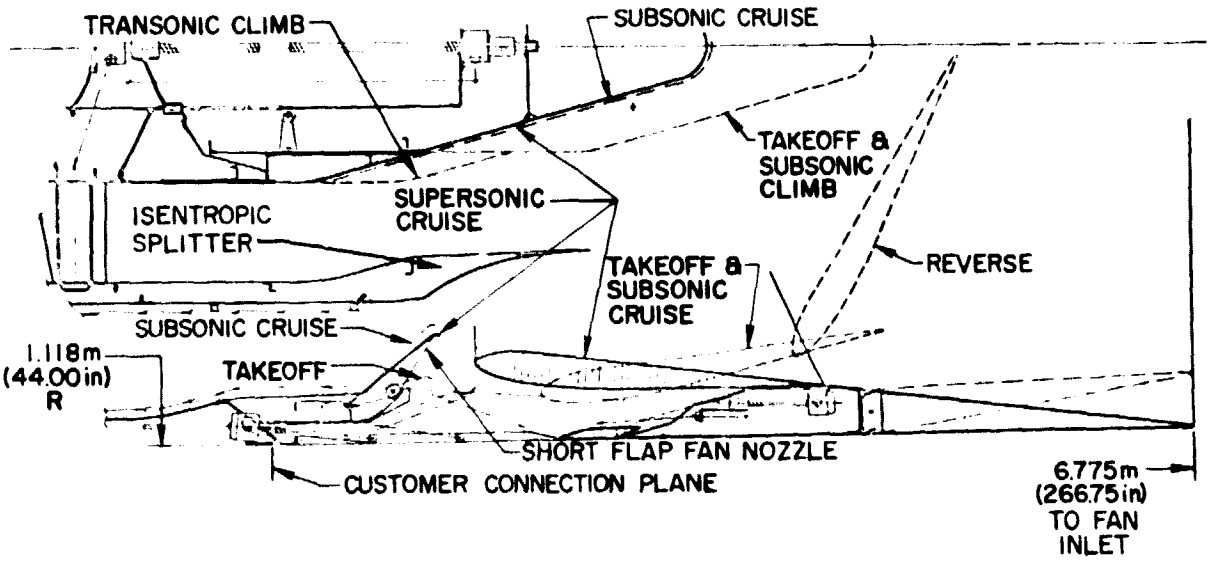

Figure 3.2-2 Short Flap Nozzle Mechanical Design Drawing

The iris nozzle has the potential for improved subsonic performance relative to the short flap configuration because there is less tendency for inlet flow separation off the longer smoother contour iris nozzle, as compared to the relatively short flap configuration. To experimentally evaluate the potential for improved subsonic performance and quantify the loss of a modest splitter flow impingement angle, the iris nozzle design of Reference 1 was modified, as shown in Figure 3.2-3. The modifications included reducing the flow splitter impingement angle to 15 degrees and incorporating the primary plug flowpath of the baseline configuration. This iris flap fan nozzle design provided a second configuration for wind tunnel evaluation.

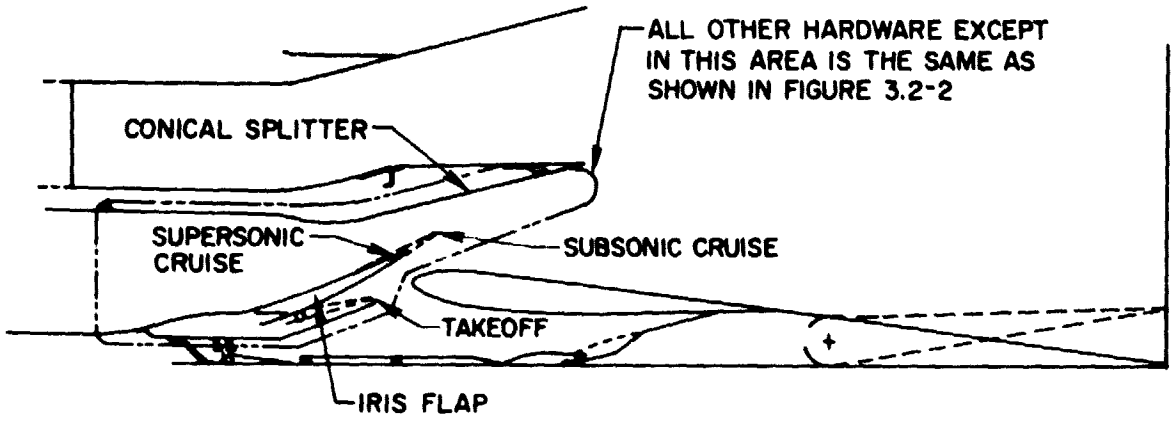

Figure 3.2-3 Iris Nozzle Mechanical Design Drawing

3.2.2 Model Design

Three 0.0966 scale model configurations of both the iris and short flap nozzle designs were fabricated for testing. The models were designed to simulate the exhaust systems operating in the takeoff, subsonic cruise, and supersonic cruise modes, as shown in Figures 3.2-4a, b and c. The principle nozzle design parameters and test variables for each operating mode, as shown in the preceding figure, are tabulated in Table 3.2-III.

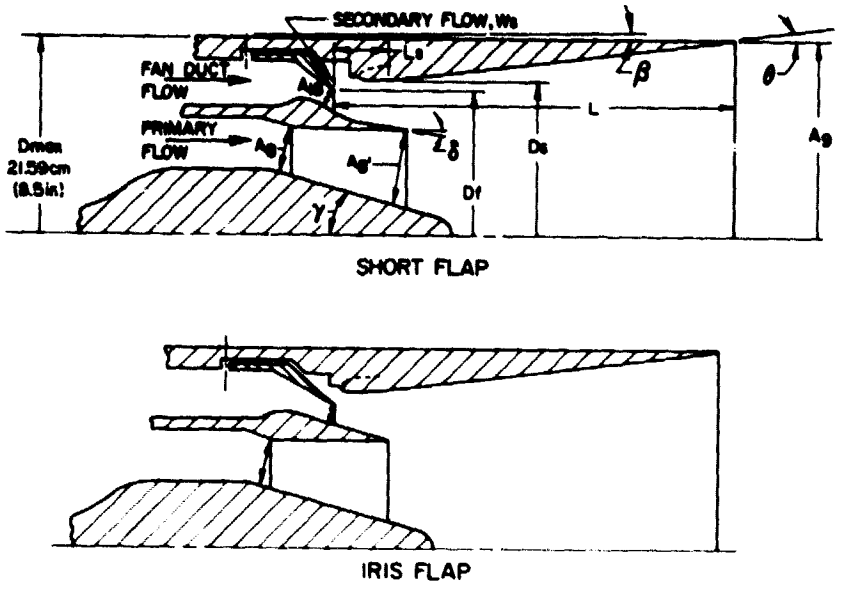

(a) Supersonic Cruise Research Model Test Configurations

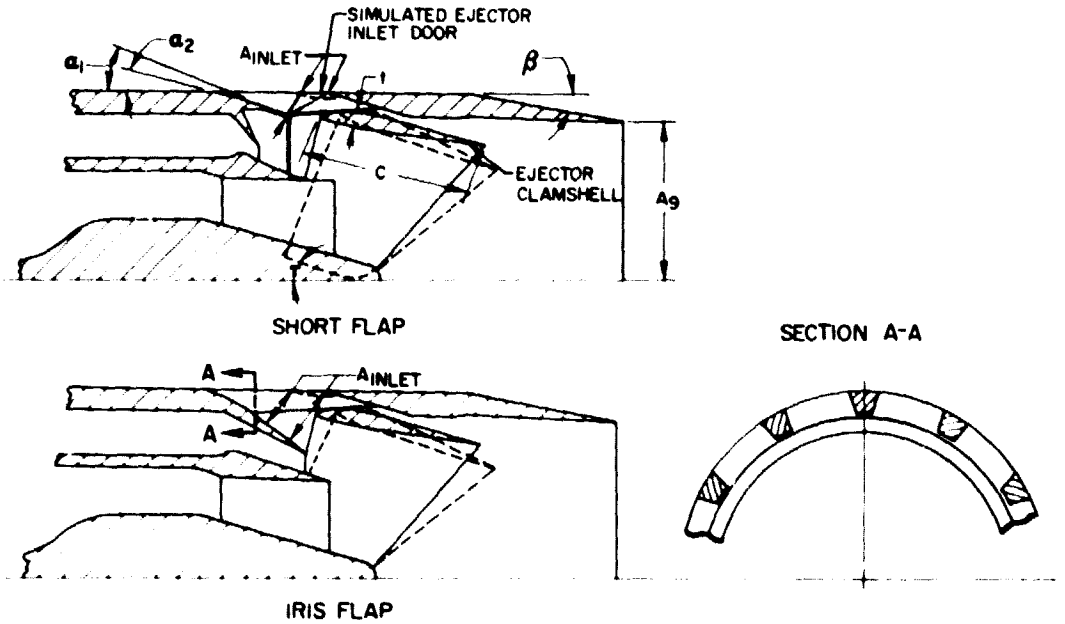

(b) Subsonic Cruise Research Model Test Configurations

Figure 3.2-4 Model Test Configurations

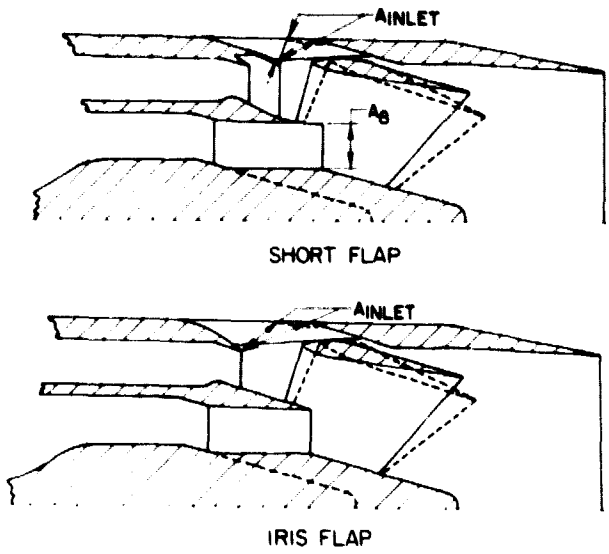

(c) Takeoff Research Model Test Configurations

Figure 3.2-4 Concluded

The research nozzle model assembly was mated to the wind tunnel jet exit model, i.e., the structure supporting the research nozzle, with the coannular adapter section shown in Figure 3.2-5. The adapter contained choke plates in the fan and primary streams to provide uniform flow approaching the charging station. The six models were designed to utilize common hardware where possible. A single primary plug with appropriate spacers served all six configurations. The conical and contoured flow splitters were common with the three iris and short flap models, respectively. Both supersonic cruise models utilized the same ejector shroud. All subsonic cruise and takeoff configurations were assembled with the same ejector shroud. Photographs of model components are presented in Figures 3.2-6 through 3.2-10. Detailed design drawings of the research nozzle model hardware are contained in the Comprehensive Data Report (Reference 5).

Secondary flow for the supersonic cruise models was provided by bleeding flow from the fan duct stream to an annulus around the fan nozzle where it flowed into the ejector shroud as shown in Figure 3.2-5. The bleed flow passed through a series of holes in the fan duct outer wall. The flow rate was set by varying the number of open holes. A separate blocker ring was designed to seal the secondary flow annulus for fan nozzle flow calibration.

Variation of the ejector inlet area was provided by axial translation of the 12 ejector inlet doors located between the shroud support stings, as shown in Figure 3.2-4, similar to the full scale design. A screw clamp arrangement held each door in a fixed axial position. At door positions other than full open, the existing gap between the door and shroud was filled to provide an aerodynamically smooth surface.

TABLE 3.2-III

PRINCIPLE NOZZLE DESIGN PARAMETERS OR VARIABLES
MODEL SCALE
REFERENCE: FIGURE 3.2-4

OPERATING MODE/CONFIGURATION	Iris	Short Flap
SUPERSONIC CRUISE		
Primary nozzle area (A_8) -- cm^2 (in^2)	74.32 (11.52)	74.32 (11.52)
Fan nozzle area (A_{18}) -- cm^2 (in^2)	47.68 (7.39)	47.68 (7.39)
Overall nozzle area ratio ($A_9/(A_8 + A_{18})$)	2.84	2.84
Primary nozzle area ratio (A_8'/A_8)	1.26	1.26
Shroud length to diameter ratio (L/D_{max})	0.98	0.98
Shroud min. diameter to fan nozzle diameter ratio (D_s/D_f)	1.11	1.08
Location of shroud min. diameter to fan nozzle diameter ratio (L_s/D_f)	0.11	0.16
Shroud external convergence angle (β) -- deg.	0.5	0.5
Shroud internal divergence (Θ)	6.3	6.3
Flow impingement angle (δ) -- deg.	13	0
Plug half-angle (γ) -- deg.	15	15
SUBSONIC CRUISE		
Primary nozzle area (A_8) -- cm^2 (in^2)	74.00 (11.47)	74.00 (11.47)
Fan nozzle area (A_{18}) -- cm^2 (in^2)	34.32 (5.32)	34.32 (5.32)
Primary nozzle area ratio (A_8'/A_8)	1.26	1.26
Overall nozzle area ratio ($A_9/(A_8 + A_{18})$)	2.35	2.35
Ejector inlet to exit area ratio (A_{inlet}/A_9)	0.56, 0.63, 0.69*	0.36, 0.46, 0.60*
Clamshell thickness to chord ratio (t/c)	0.09	0.09
Initial inlet angle (α_1) -- deg.	10	10
Final inlet angle (α_2) -- deg.	35	20
Trailing edge flap boattail angle (β) -- deg.	10	10
Clamshell angle of rotation from supersonic cruise position (τ) -- deg.	13,17,21*	13,17,21*
TAKEOFF		
Primary nozzle area plug extended (A_8) -- cm^2 (in^2)	69.83 (10.82)	69.83 (10.82)
Fan nozzle area (A_{18}) -- cm^2 (in^2)	103.23 (16.0)	103.23 (16.0)
Primary nozzle area ratio, plug retracted (A_8'/A_8)	1.37*	1.37*
Overall nozzle area ratio ($A_9/(A_8 + A_{18})$)	1.47	1.47
Ejector inlet to exit area ratio (A_{inlet}/A_9)	0.67, 0.80, 0.91*	0.36, 0.46, 0.60*
Initial inlet angle (α_1) -- deg.	10	10
Final inlet angle (α_2) -- deg	20	20
Trailing edge flap boattail angle (β) -- deg.	10	10
Clamshell angle of rotation from supersonic cruise position (τ) -- deg.	13,17,21*	13,17,21*

*Test variable

NOTE: A complete dimensional description of the model components is provided in the Comprehensive Data Report, Reference 5.

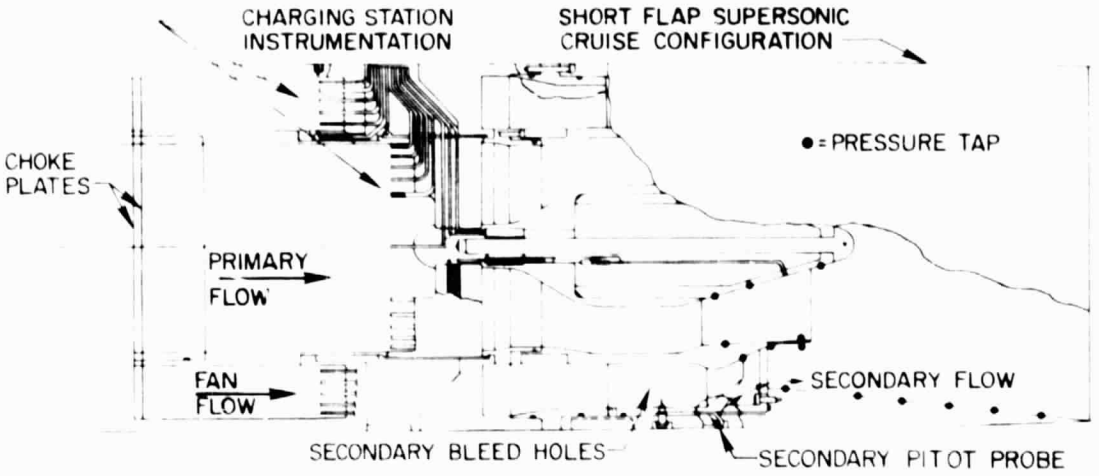

Figure 3.2-5 Typical Research Nozzle Installation on Wind Tunnel Model

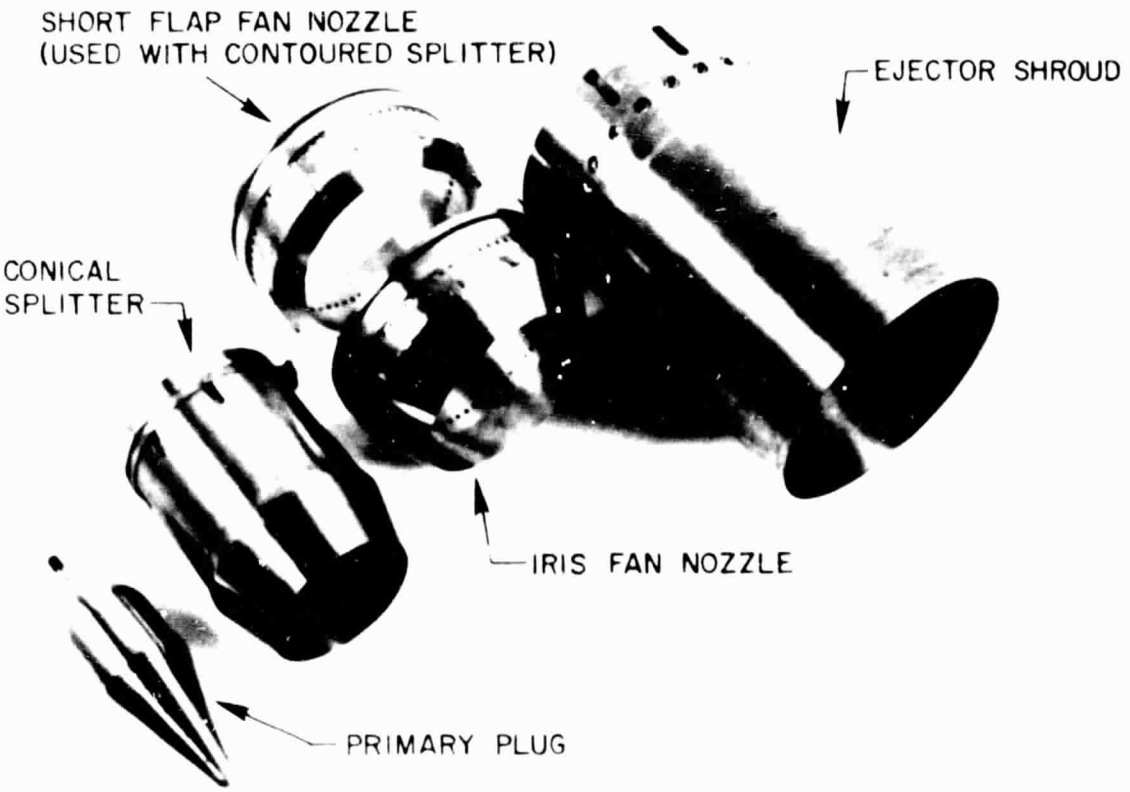

Figure 3.2-6 Supersonic Cruise Model Components

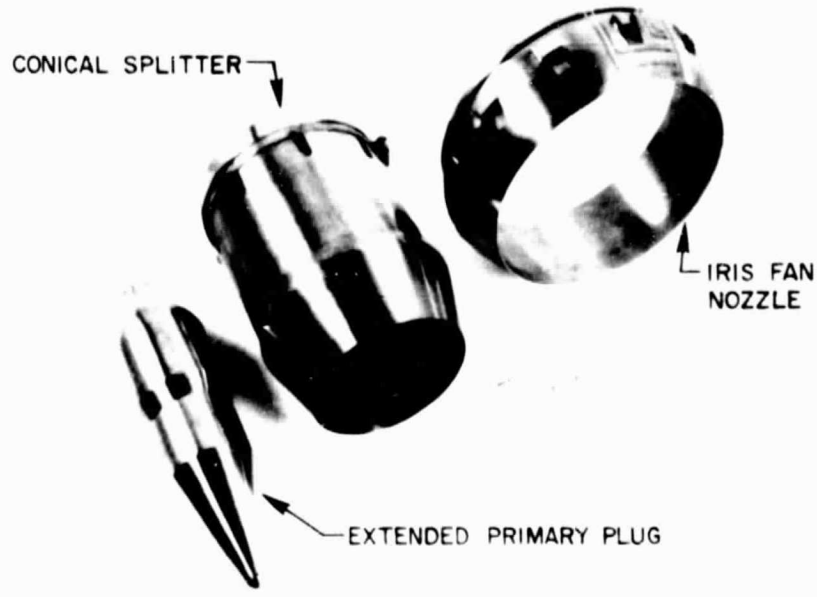

Figure 3.2-7 *Iris Nozzle Takeoff Configuration Components*

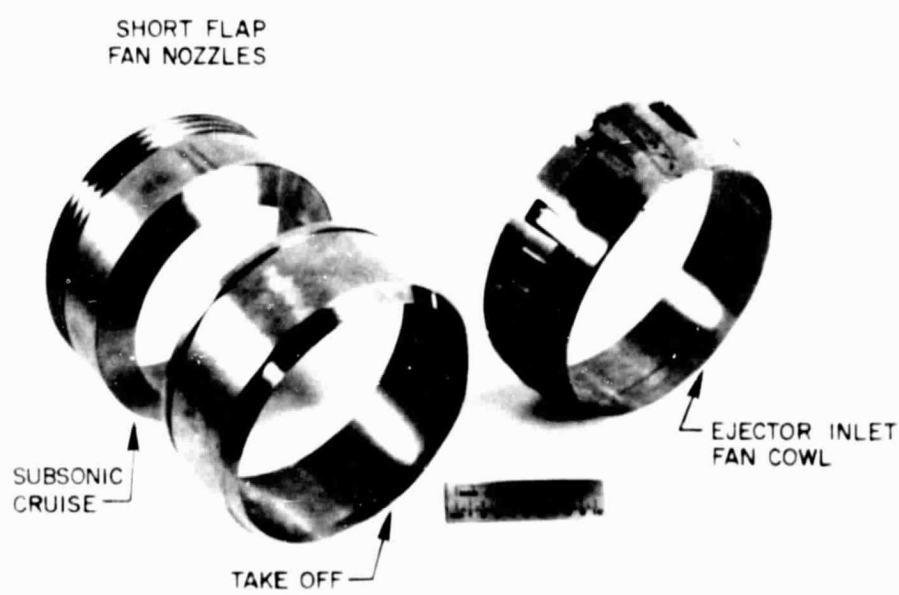

Figure 3.2-8 *Short Flap Fan Nozzle Subsonic Cruise and Takeoff Components*

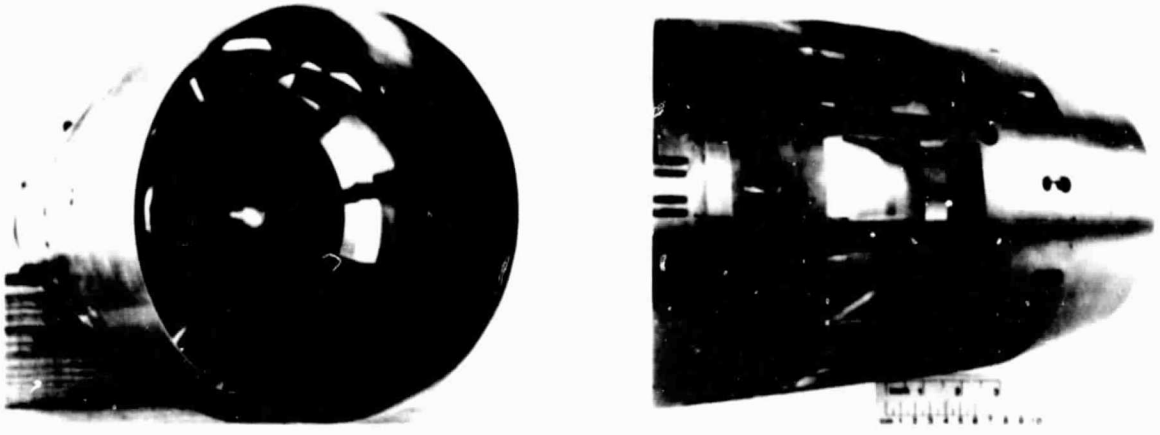

(a)END VIEW (b)SIDE VIEW

Figure 3.2-9 *Subsonic Cruise Nozzle Assembly - Iris Flap Configuration*

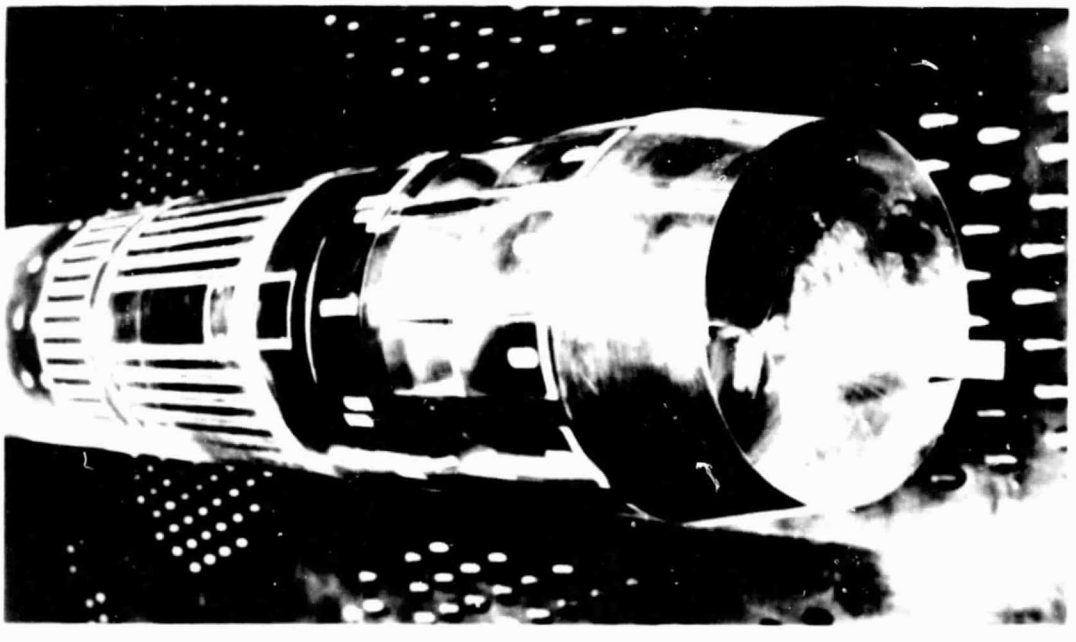

Figure 3.2-10 *Short Flap Subsonic Cruise Configuration Installed in Wind Tunnel*

Variation of the ejector clamshell position shown in Figure 3.2-4b was provided by rotating each clamshell bucket about a pivot pin located in the shroud wall, similar to the full scale design. Each clamshell segment was designed with three index holes located 90 degrees from the pivot point which engaged a locking pin extending from the shroud wall. This design allowed the clamshells to be rotated aft from the supersonic cruise position through angles of 13, 17, and 21 degrees by engaging the locking pin in the appropriate clamshell index hole.

3.2.3 Model Instrumentation

Fan and primary nozzle charging station instrumentation used to determine stream flow properties was located in the constant area sections of the model support shafting, as shown in Figure 3.2-5. The primary stream total pressure was measured with a centerline probe and two five-probe rakes at positions diametrically opposed. The probes were located at centers of equal area. Two static taps were located in the primary duct wall, each displaced 15 degrees from a primary rake. Primary total temperature was measured with a single three-probe area weighted total temperature rake. The temperature probes were constructed with chromel-alumel thermocouples. The primary stream measuring station was located 18.8 cm (7.4 in) upstream of the primary nozzle exit plane. Fan stream properties were measured with two five-probe total pressure rakes and a three-probe total temperature rake. Both pressure and temperature probes were at centers of equal area in the annular passage. The two total pressure rakes were located 180 degrees apart. Two static taps were installed in the vicinity of each total pressure rake. These taps were located in the inner and outer annulus walls and displaced 15 degrees from the rakes. The fan stream measuring station was located 25.6 cm (10.08 in) upstream of the fan nozzle exit. Secondary flow pressure was measured with two total pressure probes positioned 180 degree apart located downstream of the flow discharge annulus as shown in Figures 3.2-11a and b.

Static pressure taps were installed on the model surfaces to aid in the analysis of performance data. The location of instrumentation for each configuration is illustrated in Figures 3.2-11a through 3.2-11f and tabulated in Table 3.2-IV. The tabulated values ($X/D_{maximum}$) are referenced relative to the model connection flange and normalized by the model maximum diameter, 21.59 cm (8.5 in). During the test program, in some instances, not all of the pressure and temperature data were recorded. The instrumentation is described to indicate what information is available.

3.2.4 Test Matrix

A test matrix tabulating the combinations of aerodynamic and geometric variables tested is shown in Table 3.2-V. For each configuration tested, fan duct nozzle pressure ratio (P_{tf}/P_o) was varied over a prescribed range at fixed values of fan to primary total pressure ratio (P_{tf}/P_{tp}). The supersonic cruise configurations were also tested with three secondary flow rates ($W_{s\ corr}$) as defined by Equation 7, page 26, at each condition of fan to primary total pressure ratio.

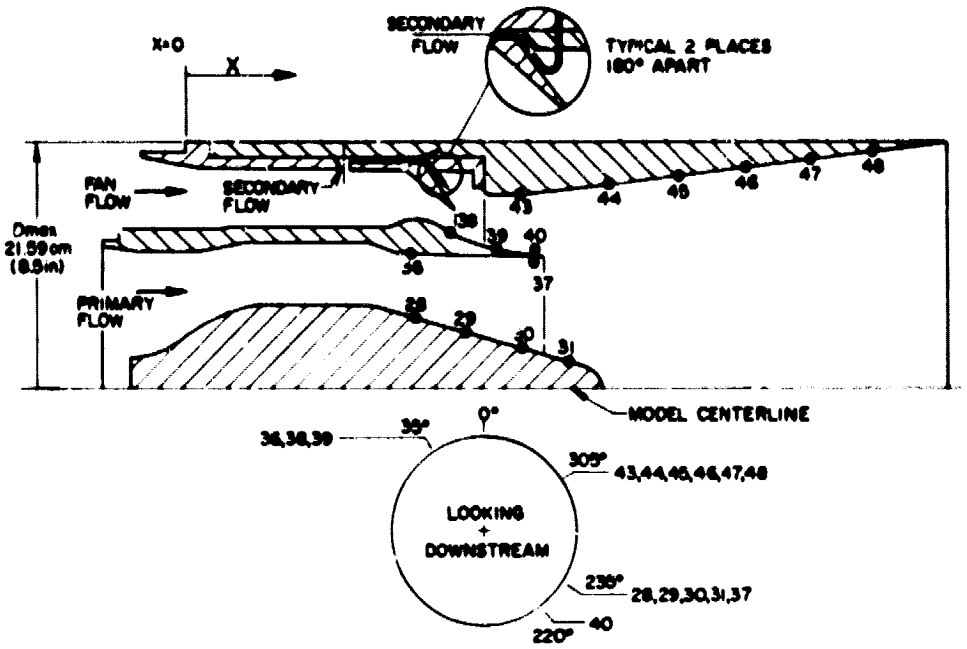

(a) Short Flap Supersonic Cruise Configuration

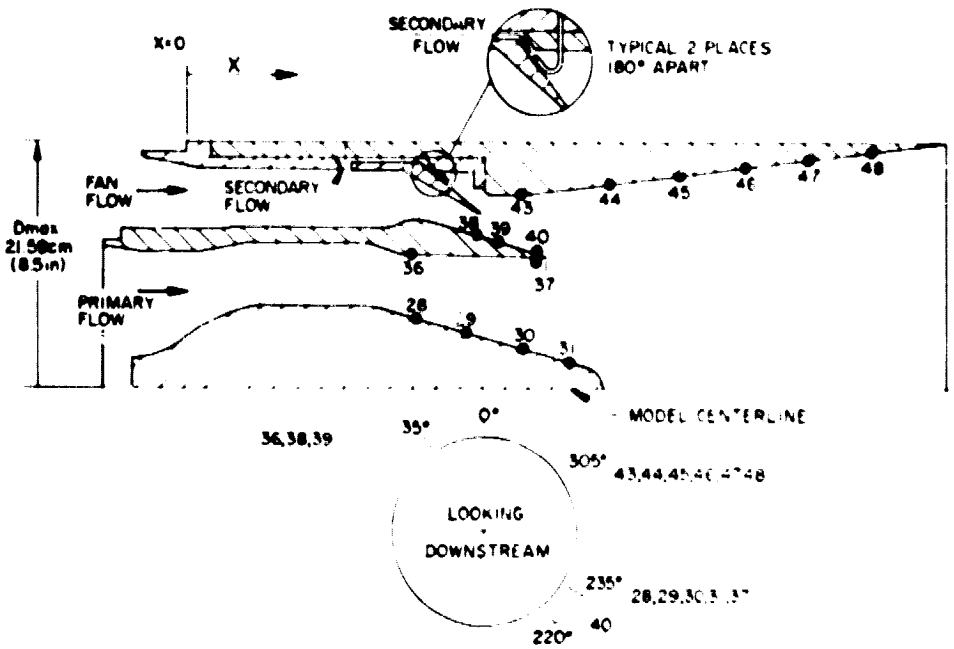

(b) Iris Supersonic Cruise Configuration

Figure 3.2-11 Static Tap Location

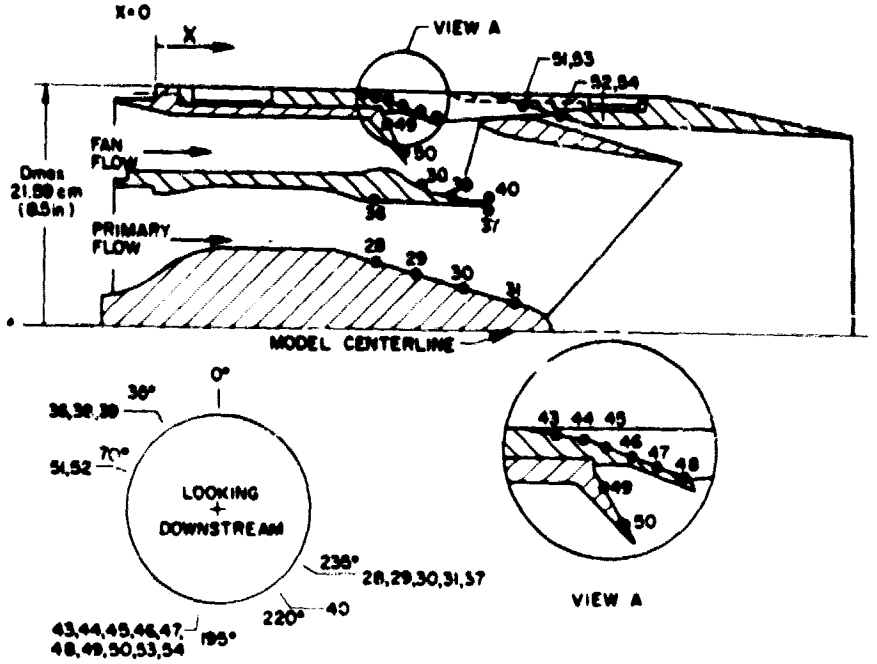

(c) Short Flap Subsonic Cruise Configuration

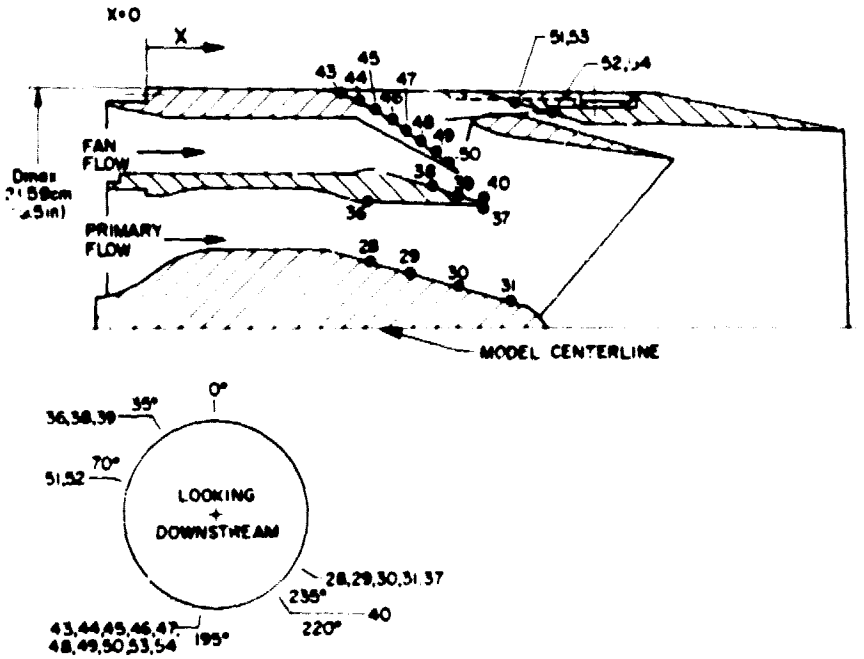

(d) Iris Subsonic Cruise Configuration

Figure 3.2-11 Static Tap Location (Cont'd)

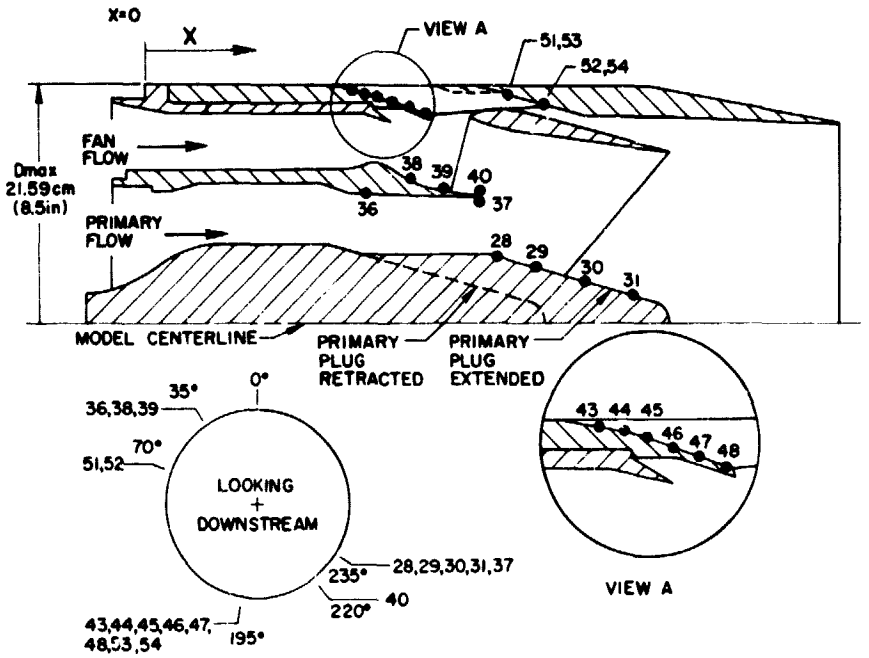

(e) Short Flap Takeoff Configuration

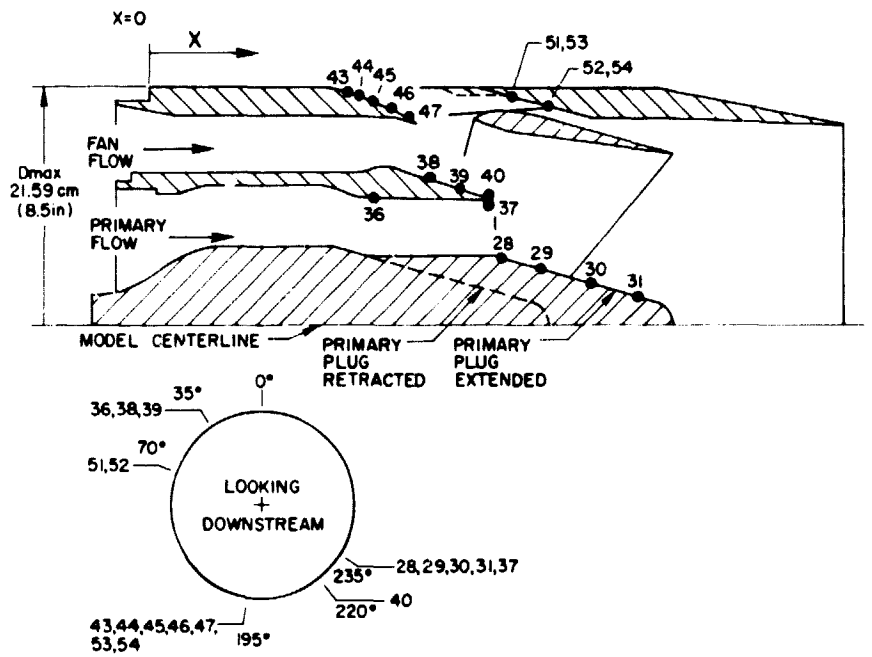

(f) Iris Takeoff Configuration

Figure 3.2-11 Static Tap Location (Concluded)

TABLE 3.2-IV

STATIC TAP LOCATION - X/D_{max}

SHORT FLAP SUPERSONIC CRUISE CONFIGURATION

Plug		Flow Splitter		Ejector	
Tap No.	X/D_{max}	Tap No.	X/D_{max}	Tap No.	X/D_{max}
28	0.432	36	0.422	43	0.624
29	0.530	37	0.670	44	0.830
30	0.629	38	0.508	45	0.960
31	0.727	39	0.583	46	1.090
		40	0.670	47	1.220
				48	1.350

Iris Supersonic Cruise Configuration

Plug		Flow Splitter		Ejector	
Tap No.	X/D_{max}	Tap No.	X/D_{max}	Tap No.	X/D_{max}
28	0.432	36	0.422	43	0.624
29	0.530	37	0.692	44	0.830
30	0.629	38	0.569	45	0.960
31	0 727	39	0.635	46	1.090
		40	0.692	47	1.227
				48	1.350

TABLE 3.2 - IV (CONTINUED)

STATIC TAP LOCATION - X/D_{MAX}

SHORT FLAP SUBSONIC CRUISE CONFIGURATION

Plug		Flow Splitter		Forebody		Fan Nozzle Flap		Ejector	
Tap No.	X/D_{max}	Tap No.	X/D_{max}	Tap No.	X/D_{max}	Tap No.	X/D_{max}	Tap No.	X/D_{max}
28	0.434	36	0.422	43	0.398	49	0.463	51	0.793
29	0.533	37	0.670	44	0.431	50	0.495	52	0.844
30	0.631	38	0.508	45	0.449			53	0.793
31	0.729	39	0.583	46	0.486			54	0.844
		40	0.670	47	0.522				
				48	0.558				

IRIS SUBSONIC CRUISE CONFIGURATION

Plug		Flow Splitter		Forebody		Ejector	
Tap No.	X/D_{max}	Tap No.	X/D_{max}	Tap No.	X/D_{max}	Tap No.	X/D_{max}
28	0.434	36	0.422	43	0.319	51	0.793
29	0.533	37	0.692	44	0.340	52	0.844
30	0.631	38	0.564	45	0.386	53	0.793
31	0.729	39	0.635	46	0.432	54	0.844
		40	0.692	47	0.478		
				48	0.522		
				49	0.563		
				50	0.605		

TABLE 3.2 - IV (Concluded)

STATIC TAP LOCATION - X/D_{MAX}

SHORT FLAP TAKEOFF CONFIGURATION

Plug Retracted		Plug Extended		Flow Splitter		Forebody		Ejector	
Tap No.	X/D_{max}	Tap No.	X/D_{max}	Tap No.	X/D_{max}	Tap No.	X/D_{max}	Tap No.	X/D_{max}
28	0.434	28	0.722	36	0.422	43	0.398	51	0.793
29	0.533	29	0.820	37	0.670	44	0.431	52	0.844
30	0.631	30	0.919	38	0.508	45	0.449	53	0.793
31	0.729	31	1.017	39	0.583	46	0.486	54	0.844
				40	0.670	47	0.522		
						48	0.558		

IRIS TAKEOFF CONFIGURATION

Plug Retracted		Plug Extended		Flow Splitter		Forebody		Ejector	
Tap No.	X/D_{max}	Tap No.	X/D_{max}	Tap No.	X/D_{max}	Tap No.	X/D_{max}	Tap No.	X/D_{max}
28	0.434	28	0.722	36	0.422	43	0.319	51	0.793
29	0.533	29	0.820	37	0.692	44	0.340	52	0.844
30	0.631	30	0.919	38	0.564	45	0.336	53	0.793
31	0.729	31	1.017	39	0.635	46	0.434	54	0.844
				40	0.692	47	0.461		

TABLE 3.2-V

SHORT FLAP TEST MATRIX

Test Condition	P_{tf}/P_o	P_{tf}/P_{tf}	W_s corr	Ejector Inlet Position - A_{inlet}/A_9	Clamshell Angle- τ^o	Primary Plug Position/ Area-A_8 $cm^2(in^2)$
Supersonic cr M_o = 2.0	20 - 30	2.0, 2.32, 2.6	0, 0.02, 0.04	-	-	Retracted/ 74.32 (11.52)
Subsonic cr M_o = 0-0.9	3.5 - 7.0	1.8, 1.97, 2.2	-	0.36, 0.46	13, 17,21, Removed	Retracted/ 74.0 (11.47)
Takeoff M_o = 0,0.36	1.8 - 4.2	1.46, 1.7	-	0.36, 0.46, 0.60	13, 17, 21 Removed	Retracted/ 69.83 (10.82)
						Extended/ 69.83 (10.82)

IRIS NOZZLE TEST MATRIX

Test Condition	P_{tf}/P_o	P_{tf}/P_{tf}	W_s corr	Ejector Inlet Position - A_{inlet}/A_9	Clamshell Angle- τ^o	Primary Plug Position/ Area-A_8 $cm^2(in^2)$
Supersonic cr M_o = 2.0	20 - 30	2.0, 2.32, 2.6	0, 0.02, 0.04	-	-	Retracted/ 74.32 (11.52)
Subsonic cr M_o = 0.9	3.5 - 7.0	1.8, 1.97, 2.2	-	0.42*, 0.63	21, removed	Retracted/ 74.0 (11.47)
Takeoff M_o = 0, 0.36	1.8 - 4.2	1.46, 1.7	-	0.80	13, removed	Extended/ 69.83 (10.82)
						Retracted/ 69.83 (10.82)

* Model inlet area reduced by extension of inlet door.

SECTION 4.0

DATA REDUCTION PROCEDURES

General descriptions of the equations used to define model flow rates and nozzle thrust are contained in this section. All constants and equations are given as actually used in the data reduction process.

4.1 FAN AND PRIMARY FLOW RATES

As previously discussed, both fan and primary mass flow rates were measured with a choked venturi. These flow rates were calculated using the measured air total temperature (T_{tv}) and pressure (P_{tv}), respectively, and Equation (1).

$$m_v = C_{Dv} \frac{K_v P_{tv} A_v}{\sqrt{T_{tv}}} \tag{1}$$

where: C_{Dv} is the venturi discharge coefficient, K_v the critical flow factor, and A_v the geometric throat area of the venturi.

The venturi discharge coefficient is based on analytical techniques for choked venturis with circular arc throats. This coefficient accounts for viscous effects and sonic line distortion at the venturi throat. The critical flow factor (K_v) is a function of total pressure and temperature, and accounts for real gas effects. The critical flow factor was obtained by curve-fitting tabulated values from Reference 7.

Total pressure (P_{tv}) was determined by measuring the static pressure (P_v) upstream of the venturi throat and calculating the total pressure as:

$$P_{tv} = P_v/C \tag{2}$$

The factor C is a constant for a given venturi and is the one-dimensional static to total pressure ratio corresponding to the ratio of the area at the measuring plane to the venturi throat area. The static pressure was measured by four taps, each of which was sampled six times with a 48-channel signal commutator for each data point. These 24 readings were averaged to determine the static pressure. Venturi total temperature (T_{tv}) was determined using three iron/constantan thermocouples located upstream of each venturi, with the readings averaged.

4.2 DISCHARGE COEFFICIENTS

The discharge coefficient of a nozzle is defined as the ratio of actual mass flow through the nozzle to the ideal isentropic flow rate at the temperature and pressure of the flow (Equation 3).

$$C_D = \frac{m}{m_i} \tag{3}$$

Ideal flow rate was calculated from the following equation:

$$m_i = \frac{K P_t A}{\sqrt{T_t}} \left(\frac{A^*}{A} \right) \tag{4}$$

where: A, P_t, and T_t are the nozzle geometric throat area, total pressure, and total temperature, respectively.

The critical flow factor (K) is a function of nozzle total pressure and temperature and was obtained by curve-fitting tabulated values from Reference 7. Area ratio A*/A is the ratio of flow area at sonic conditions to the nozzle throat area. For values of nozzle pressure ratio (P_t/P_o) greater than 1.8929, A*/A in the ideal weight flow equation is equal to one. For lower pressure ratios, A*/A was calculated from one-dimensional, isentropic relationships:

$$A^*/A = \frac{216}{125} M \left(1 + \frac{M^2}{5} \right)^{-3} \tag{5}$$

where

$$M = \left\{ 5 \left[\left(P_t/P_o \right)^{0.28571} - 1 \right] \right\}^{1/2} \tag{6}$$

4.3 SECONDARY FLOW RATE AT SUPERSONIC CRUISE

Secondary flow ($W_{s\ corr}$) was introduced into the ejector for some supersonic cruise test conditions. Corrected secondary flow is defined as the ratio of the temperature-corrected secondary bleed flow relative to the temperature-corrected sum of the fan and primary nozzle flows, as expressed by the following equation:

$$W_{s\ corr} = \frac{m_s \sqrt{T_{ts}}}{m_f \sqrt{T_{tf}} + m_p \sqrt{T_{t_p}}} \tag{7}$$

For tests of the supersonic cruise configurations, secondary flow was bled from the fan duct upstream of the nozzle throat. Since the total temperature of all the streams in the model tests were equal, flow temperature corrections were not required.

The secondary mass flow (m_s) was calculated using the following relations:

$$m_s = \Delta C_{Df}\ m_{if} \tag{8}$$

where

$$\Delta C_{Df} = (C_{Df})_{\substack{\text{with} \\ \text{secondary} \\ \text{flow}}} - C_{Df} \tag{9}$$

The fan nozzle discharge coefficient (C_{D_f}) was determined at supersonic cruise with no secondary flow by using the equations in the previous section. Once the fan nozzle discharge coefficient was determined for a given nozzle, calibrations were conducted to determine the fan nozzle discharge coefficient with secondary flow. Since the secondary flow was bled from the fan duct upstream of the nozzle, the discharge coefficient increased (i.e., high calculated fan flow rate (m_f) relative to fan ideal flow rate (m_{if})). This apparent increase in flow was correlated with the number of open bleed holes. Thus, to obtain a specified level of secondary flow during the actual test, the required number of bleed holes was opened and Equation (8) was used to determine m_s.

To account for the fact that secondary flow was bled from the fan stream, the equation for determining fan flow rate was modified as follows:

$$m_f = C_{Dvf} \frac{K_{vf} P_{tvf} A_{vf}}{\sqrt{T_{tvf}}} - m_s \qquad (10)$$

4.4 SECONDARY TOTAL PRESSURE ADJUSTMENT

Because of an instrumentation problem with the iris supersonic cruise configuration, the measured secondary total pressure (P_{ts}) at 4 percent secondary flow was determined invalid. It therefore became necessary to adjust this questionable pressure based on calibrations of valid secondary total pressure measurements and secondary flow rate. In the correlation, it was assumed that the secondary flow passage was choked, as discussed in Section 5.1.1, and that one dimensional, isentropic flow conditions existed.

At test conditions where valid secondary total pressure measurements were obtained, a choked flow area was calculated using measured secondary total pressure, temperature, and weight flow. For each nozzle configuration, this calculated area was found to be almost constant over the entire range of test conditions. For example, the area for the iris nozzle with 2 percent secondary flow varied no more than 0.7 percent from the average for the 30 test cases. The average calculated area for this case was found to differ by only 3.3 percent from the comparable area for a similar nozzle with 2 percent secondary flow. The choking flow area for the iris nozzle with 4 percent flow was determined by assuming that the same relationship existed at this flow condition, i.e., the same proportionality was assumed at 4 percent as existed at 2 percent flow. With this calculated area, as well as measured weight flow and temperature, it was then possible to calculate the secondary pressure for the iris nozzle with 4 percent secondary flow for each test case of interest. The resulting variation in secondary pressure was found very similar to that observed for the other nozzles. Thus, the calculated pressure is believed to be valid for analysis of the test results.

4.5 THRUST MEASUREMENTS

For this test, the nozzle generated thrust-minus-drag is defined as the axial exit momentum of the exhaust flow, plus the excess of exit pressure over ambient pressure times the exit area normal to the axis, minus the axial pressure drag on the nozzle external surfaces (i.e., trailing edge flaps and auxiliary inlet doors).

$$F - D_{ex} = \int_{A_{exit}} d(mV)_{axial} + \int_{A_{exit}} (P_{exit} - P_o)dA - D_{ex} \tag{11}$$

Thus, this definition of thrust-minus-drag does not penalize the nozzle for external friction drag.

Figure 4.1 shows a control volume applied to the test nozzles. Writing the momentum equation in the axial direction for this control volume demonstrates how the thrust was measured for this test:

$$F_{LC} + \Sigma P_{int} A_{int} - P_{exit} A_{exit} + D_{sm} + D_{ex} = mV_{exit} \tag{12}$$

Substituting Equation (11) for mV_{exit} in Equation (12) then,

$$F_{LC} + \Sigma P_{int} A_{int} - P_{exit} A_{exit} + D_{sm} + D_{ex} = (F-D_{ex}) - (P_{exit} - P_o) A_{exit} + D_{ex} \tag{13}$$

Rearranging and cancelling terms,

$$F-D_{ex} = F_{LC} + \Sigma P_{int} A_{int} - P_o A_{exit} + D_{sm} \tag{14}$$

But

$$P_o A_{exit} = \Sigma P_o A_{int} \tag{15}$$

Therefore

$$F-D_{ex} = F_{LC} + \Sigma A_{int} (P_{int} - P_o) + D_{sm} \tag{16}$$

F_{LC} is the axial force measured by the load cell, which was calibrated by applying a known force and correlating this force against the load cell output. Thus, this calibration provided a linear relationship between the applied load and the load cell output in millivolts, which was used to determine the load cell force

$$F_{LC} = a(m_v) + b \tag{17}$$

where a and b are constants determined by the calibrations and m_v is the load cell reading in millivolts. The load cell was sampled 26 times for each test condition, the above calculation was made for each sample, and the results averaged to yield the measured force.

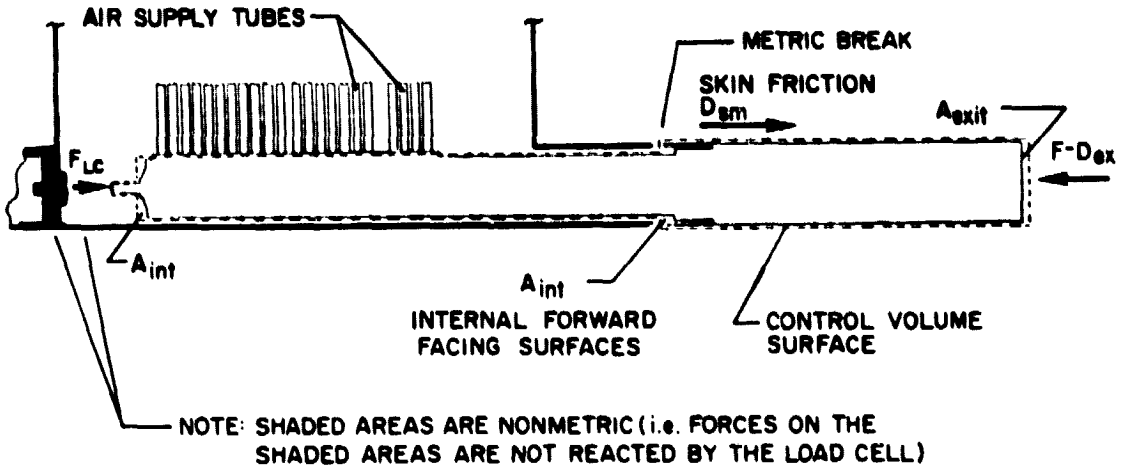

Figure 4-1 *Control Volume for 21.59 cm (8.5 in.) Model Thrust Determination*

The term A_{int} (P_{int} - P_o) accounts for internal pressure tare forces acting on the forward facing surfaces (A_{int}) of the metric part of the model. The internal pressure (P_{int}) was measured with two static pressure taps 180-degrees apart at each of the forward facing surfaces.
As indicated by Equation (16), an adjustment was made to the measured thrust-minus-drag of the nozzles to account for external skin friction drag (D_{sm}) acting on the cylindrical section of the model downstream of the metric break. External skin friction drag was estimated by using the method reported in Reference 8.

4.6 THRUST COEFFICIENTS

The gross thrust coefficient is defined as the ratio of measured nozzle gross thrust-minus-drag to the sum of the ideal thrusts of the fan and primary streams. As noted previously, the thrust-minus drag for this report does not penalize the nozzle for external skin friction drag. Ideal thrust for each stream equals the mass flow rate times the ideal velocity, i.e., the velocity of the stream expanded isentropically from the upstream total pressure to the ambient pressure. The equation for the gross thrust coefficient is thus:

$$C_{fp} = \frac{F - D_{ex}}{\dot{m}_f V_{if} + \dot{m}_p V_{ip}} \qquad (18)$$

The ideal thrust for each stream was calculated using the dimensionless ideal thrust function, which is a function of nozzle pressure ratio (P_t/P_o) and the ratio of specific heats γ.

$$\frac{m_i V_i}{P_t A^*} = \gamma \left(\frac{2}{\gamma+1}\right)^{\frac{\gamma}{\gamma-1}} \left(\frac{\gamma+1}{\gamma-1}\right)^{1/2} \left[1 - (P_o/P_t)^{\frac{\gamma-1}{\gamma}}\right]^{1/2} \quad (19)$$

$$\text{or} \quad \frac{m_i V_i}{P_t A^*} = 1.81163 \sqrt{1 - (P_o/P_t)^{.28571}} \quad \text{for } \gamma = 1.4 \quad (20)$$

The ideal thrust for the fan and primary streams was then:

$$m_f V_{if} = C_{Df} Pt_f A_f \left(\frac{A^*}{A}\right)_f \left(\frac{m_i V_i}{P_t A^*}\right)_f \quad (21)$$

$$m_p V_{ip} = C_{Dp} Pt_p A_p \left(\frac{A^*}{A}\right)_p \left(\frac{m_i V_i}{P_t A^*}\right)_p \quad (22)$$

For pressure ratios greater than 1.8929, A*/A = 1.0. For pressure ratios less than this, A*/A was calculated as described in the previous section on discharge coefficients.

4.7 NOZZLE EFFICIENCY

In addition to nozzle gross thrust coefficient, a nozzle efficiency coefficient, η , was also defined, which relates the overall efficiency of the exhaust system by including the ideal thrust contribution of the secondary flow, as follows:

$$\eta = \frac{F - D_{ex}}{m_f V_{if} + m_p V_{ip} + m_s V_{is}} \quad (23)$$

where $m_f V_{if}$ and $m_p V_{ip}$ were calculated using Equations (21) and (22). Since a discharge coefficient was not calculated for the secondary flow, the following equation was used to calculate $m_s V_{is}$:

$$m_s V_{is} = m_s \sqrt{\left(\frac{2\gamma}{\gamma-1}\right) gRT_{ts} \left[1 - \left(\frac{P_o}{Pt_s}\right)^{\frac{\gamma-1}{\gamma}}\right]} \quad (24)$$

rearranging and setting $\gamma = 1.4$,

$$m_s V_{is} = 2.64575\, m_s \sqrt{gRT_{ts} \left[1 - \left(\frac{P_o}{Pt_s}\right)^{.28571}\right]} \quad (25)$$

SECTION 5.0

RESULTS AND DISCUSSION

The measured nozzle thrust performance and exhaust flow characteristics of the two nozzle configurations tested, the iris and the short flap design, are presented in this section. Included are the effects of geometric and aerodynamic test variables at the simulated flight Mach numbers. Also, measured performance is compared to levels assumed for the Advanced Supersonic Transport propulsion studies. Emphasis is placed on the performance observed at simulated engine operating conditions.

In the following discussion, the thrust performance characteristics of the supersonic cruise nozzle configuration are presented first, followed by the performance of the subsonic cruise and takeoff configurations. Nozzle flow characteristics are then addressed in the same order.

5.1 NOZZLE THRUST PERFORMANCE

Two nozzle parameters are used to express thrust performance: gross thrust coefficient (C_{fp}) and nozzle efficiency coefficient (η), as defined by data reduction equations 18 and 23, respectively. It should be noted that the thrust performance described by both coefficients does not penalize the nozzle for external skin friction drag. Also, the thrust contribution of the secondary flow is not included in the ideal thrust terms of the gross thrust coefficient (C_{fp}).

5.1.1 Supersonic Cruise Performance at Mach Number 2.0

Nozzle performance in terms of gross thrust (C_{fp}) versus fan nozzle pressure ratio (P_{tf}/P_o) is presented in Figures 5.1-1a and b for the iris and short flap configurations. In this series of curves, data are compared at three fan to primary pressure splits (P_{tf}/P_{tp}). The data were acquired at a secondary flow rate ($W_{s\ corr}$) of 2 percent. It may be observed that with the presence of secondary flow, the performance coefficient (C_{fp}) exceeds unity. As noted previously in the definition of gross thrust coefficient, the measured thrust contribution of the secondary stream is not normalized by the ideal thrust of the stream. The comparisons show that for both configurations the range of fan to primary pressure split tested had little influence on nozzle performance. Data acquired at the other secondary flow conditions, flow rates of zero and 4 percent and tabulated in the companion Comprehensive Data Report (Reference 5), also indicate that the fan to primary pressure split had a negligible effect on performance. These results suggest that if engine operation deviates somewhat from the predicted pressure split of 2.32 at supersonic cruise, nozzle performance will not be degraded.

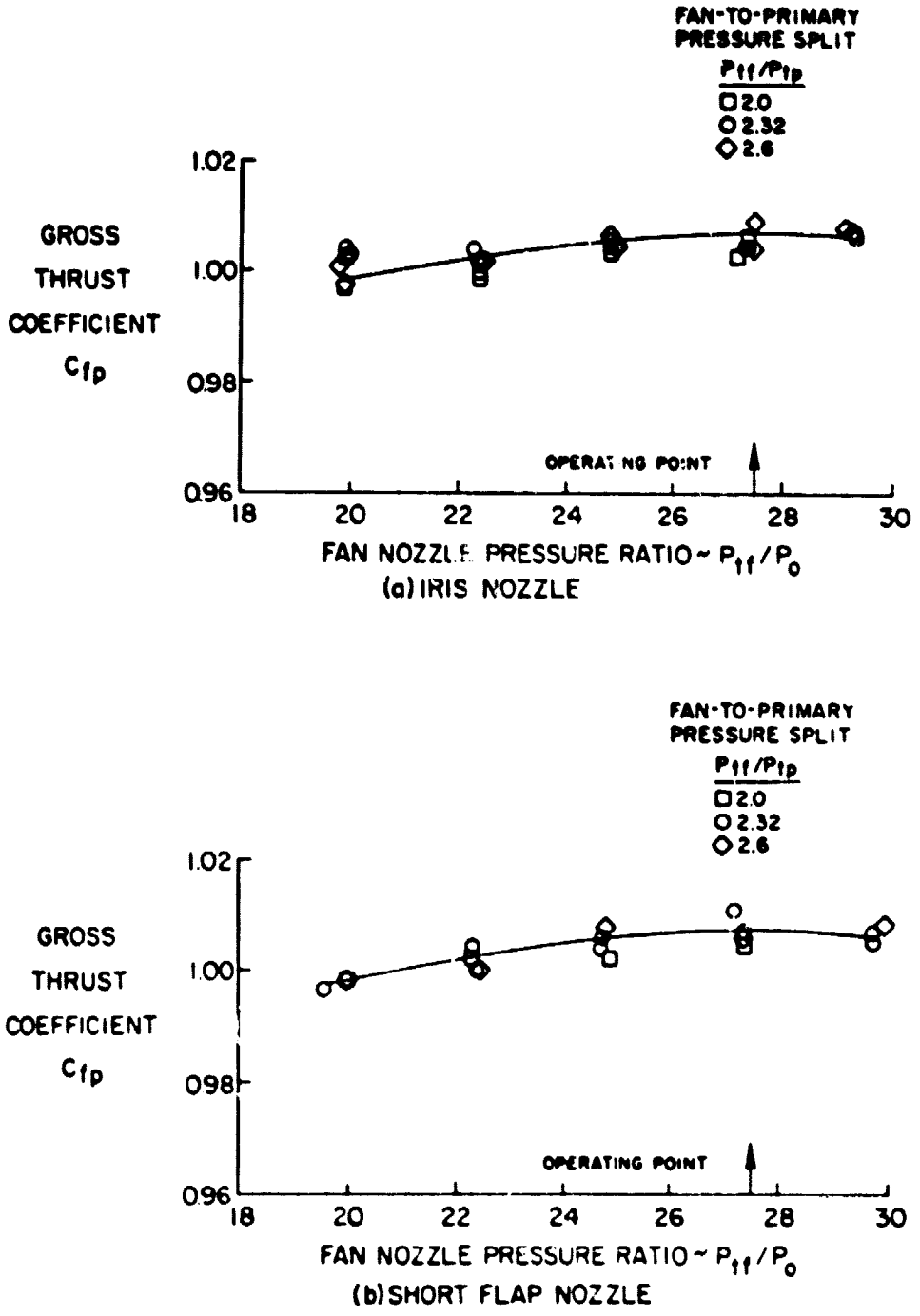

Figure 5.1-1 Comparison of Thrust Performance for Various Fan-to-Primary Pressure Splits. Conditions: Free Stream Mach Number, (M_0), 2.0; Secondary Flow, $W_{s\ corr}$, 2.0%.

The influence of secondary flow on supersonic cruise gross thrust coefficients for both configurations is shown in Figure 5.1-2. The data show that over the range of fan nozzle pressure ratios tested, the performance of the iris nozzle benefits more with increasing secondary flow in comparison to the short flap configuration. At zero secondary flow, the gross thrust coefficient of the iris nozzle is 0.4 percent less than the short flap, while at 4 percent secondary flow performance of the iris configuration is 0.2 percent higher than the short flap. Figure 5.1-2 also indicates that for zero and 2 percent secondary flow peak nozzle performance (minimum over or under-expansion losses) occurs over a fan pressure ratio range of 27 to 28. This range of measured maximum performance brackets the engine operating conditions at supersonic cruise, a fan nozzle pressure ratio of 27.5 and a fan-to-primary pressure split of 2.32 as shown in Table 3.2-I. The trend at 4 percent corrected secondary flow indicates that nozzle performance is still increasing slightly at the facility pressure limit, a fan nozzle pressure ratio of 30. For secondary flows greater than 2 percent, some allowance in area ratio must be made to achieve peak performance at the design nozzle pressure ratio.

A comparison of nozzle performance as a function of secondary flow at the supersonic cruise engine operating conditions outlined above is shown in Figure 5.1-3. The data trend indicates that small amounts of secondary flow provide a greater increase in nozzle performance than the percent mass flow added. As indicated previously, the nozzle coefficient C_{fp} does not include the ideal thrust of the secondary flow. An increase in secondary flow from zero to 2 percent increased the iris nozzle performance 2.6 percent, and the short flap nozzle 2.3 percent. A further increase in secondary flow to 4 percent showed an additional 1.5 percent improvement in iris nozzle performance and 1.2 percent for the short flap configuration. The reason for the performance increase for small additions of secondary flow is attributed to control of the initial overexpansion of the fan nozzle jet flow prior to attachment on the ejector shroud wall. At higher secondary flows, diminishing performance returns are realized.

The level of secondary total pressure (P_{ts}) required to provide a given secondary flow rate is directly proportional to the fan nozzle total pressure (P_{tf}), once compound choking flow conditions have been established for the two streams. The data in Figure 5.1-4 illustrate this correlation for the short flap nozzle by showing secondary to fan total pressure ratio (nozzle pumping characteristic), (P_{ts}/P_{tf}), as a function of fan nozzle pressure ratio. The data show that primary nozzle operating conditions have no effect on the pumping characteristic, as indicated by the collapse of data measured over a wide range of fan to primary pressure split at constant corrected secondary flow rate.

A comparison of pumping characteristics of the iris and short flap configurations tested over a range of corrected secondary flow rates (Figure 5.1-5) shows that this parameter is dependent on the nozzle geometry. As both configurations were tested with the same ejector, the difference in nozzle pumping characteristic level between the two configurations is attributed to the variance of the fan nozzle design, i.e., isentropic versus conical contoured flow splitter. Previous experience indicates that the pumping characteristic is influenced by the nozzle shape as well as the spacing between the fan nozzle and ejector shroud minimum diameter.

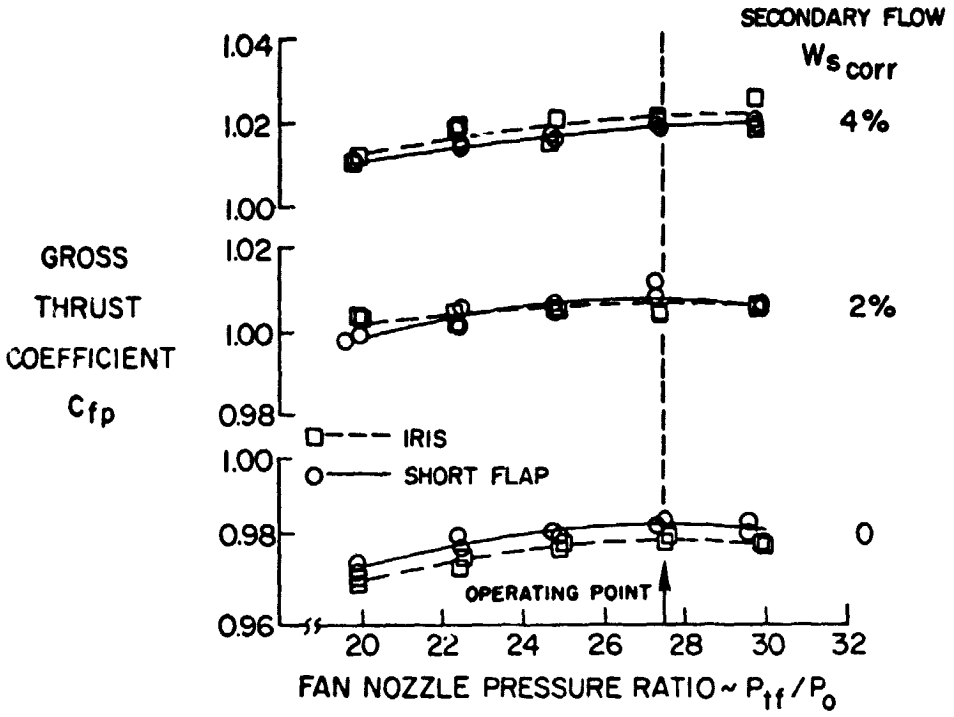

Figure 5.1-2 Comparison of Short Flap and Iris Nozzle Thrust Performance at Secondary Flow Rates of 0, 2 and 4 Percent. Conditions: Free Stream Mach Number, (M_o), 2.0; Fan-to-Primary Pressure Split, P_{tf}/P_{tp}, 2.32.

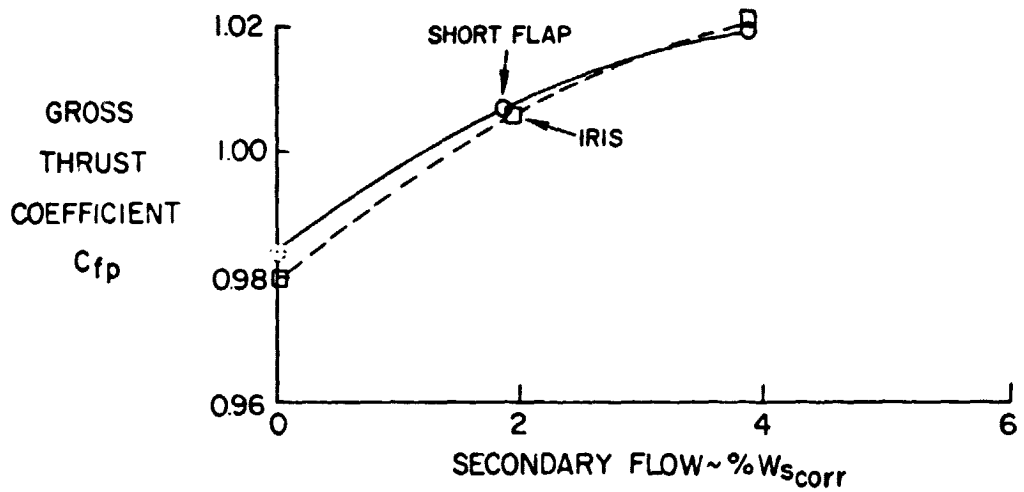

Figure 5.1-3 Effect of Secondary Flow on Nozzle Thrust Performance at Supersonic Cruise Operating Conditions. Conditions: Free Stream Mach Number, (M_o),2.0; Fan Nozzle Pressure Ratio, P_{tf}/P_o, 27.5; Fan-to- Primary Pressure Split, P_{tf}/P_{tp}, 2.32.

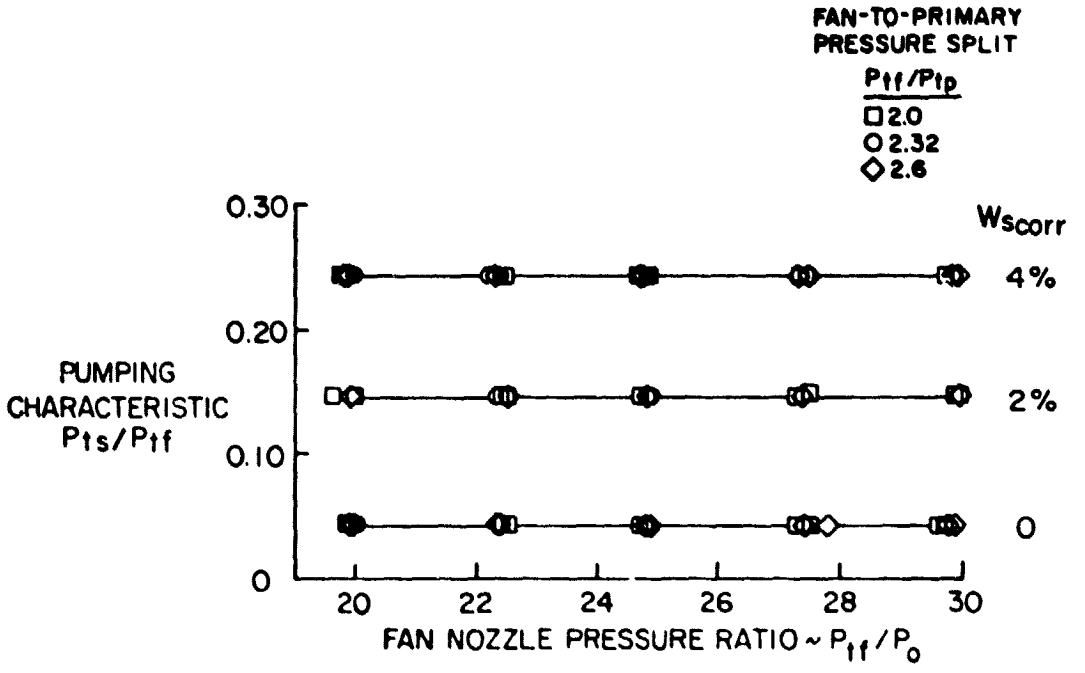

Figure 5.1-4 *Effect of Fan Nozzle Pressure Ratio on Short Flap Nozzle Pumping Characteristics. Condition: Free Stream Mach Number, (M_o) 2.0.*

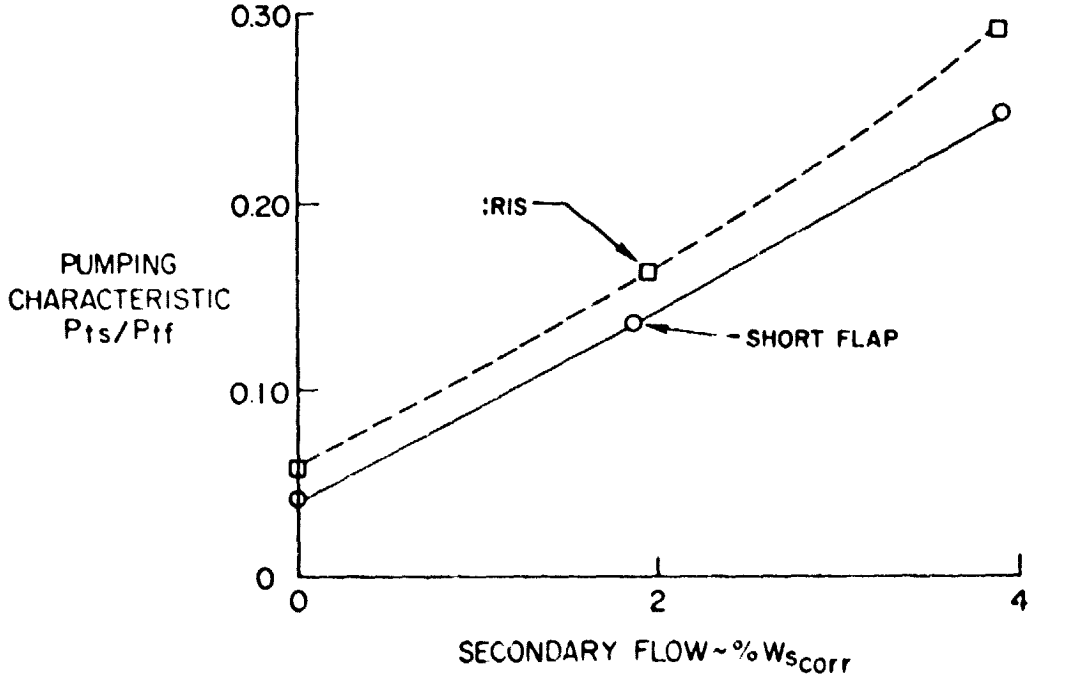

Figure 5.1-5 *Comparison of Iris and Short Flap Nozzle Pumping Characteristics. Conditions: Free Stream Mach Number, (M_o) 2.0; Fan Nozzle Pressure Ratio, P_{tf}/P_o, 27.5; Fan-to-Primary Pressure Split, P_{tf}/P_{tp}, 2.32.*

In the definition of gross nozzle thrust coefficient, the ideal thrust of secondary flow is not considered, as previously noted, because of the difficulty in accurately defining the secondary total pressure entering the ejector in full scale flight hardware and, therefore, the performance of the propulsion system. However, a definition of the level of secondary total pressure and corrected flow is necessary to provide design requirements for sizing the flow supply piping and identifying the source, i.e., inlet flow, inlet boundary layer bleed, or engine bleed.

To quantify the ejector nozzle thrust performance in terms of the ideal thrust of the total exhaust flow, primary plus fan plus secondary, the nozzle efficiency (η) was defined, as discussed earlier, Page 31. As in the gross thrust coefficient definition, nozzle efficiency does not include the effect of external skin friction drag. This definition of nozzle performance provides a convenient means of comparing ejector nozzle performance with secondary flow to the thrust coefficients of other exhaust systems that are based on the ideal thrust of the total exhaust flow expanded to ambient.

A comparison of the iris and short flap nozzle efficiencies at supersonic cruise engine operating conditions is presented in Figure 5.1-6. This comparison shows that at secondary flow rates up to 4 percent the overall performance of the short flap nozzle is superior to the iris configuration.

Data trends indicate that secondary flow rates of only 2 percent are required to obtain maximum nozzle performance. With further increases in corrected secondary flow, performance tends to fall off. At approximately 2 percent corrected secondary flow, the short flap nozzle achieves maximum performance of 0.995 and the maximum for iris configuration is 0.990.

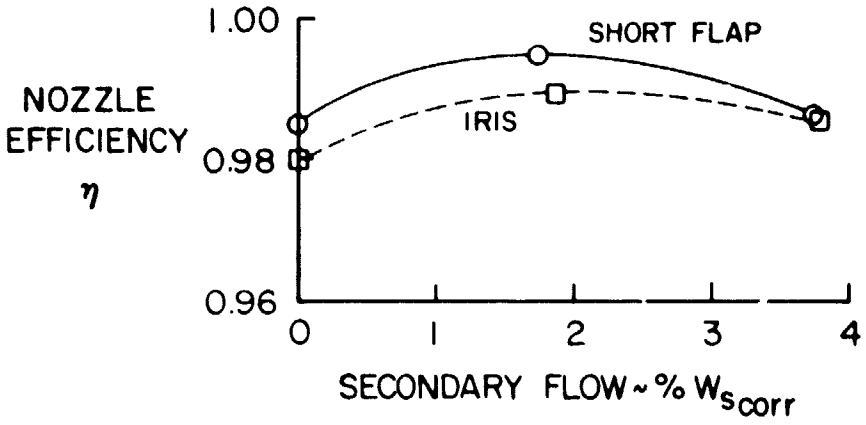

Figure 5.1-6 Comparison of Short Flap and Iris Nozzle Efficiency at Supersonic Cruise Engine Operating Conditions. Conditions: Free Stream Mach Number, (M_O) 2.0; Fan Nozzle Pressure Ratio, P_{tf}/P_O, 27.5; Fan-to-Primary Pressure Split, P_{tf}/P_{tp}, 2.32.

It is interesting to note that in terms of gross thrust coefficient at 2 percent corrected secondary flow (Figure 5.1-3), performance is nearly identical. In terms of efficiency at 2 percent corrected secondary flow, the performance of the short flap is clearly 0.5 percent higher than the iris. The reason for this apparent anomaly is that the iris configuration requires a higher secondary total pressure to pass a given secondary flow than does the short flap. The higher secondary total pressure of the iris, for a given flow, manifests itself in a proportionately larger ideal secondary thrust term relative to the short flap. As the measured thrust of both configurations is similar, the larger total ideal thrust of the iris due to the higher secondary total pressure results in a lower overall nozzle efficiency.

5.1.2 Subsonic Cruise Performance (Mach Number 0.9)

Curves of gross thrust coefficient versus fan nozzle pressure ratio are presented in Figures 5.1-7a and b comparing data at three fan-to-primary pressure splits for the subsonic cruise iris and short flap configurations. The iris nozzle data were obtained with the clamshell set at 21 degrees and an ejector inlet-to-exit area ratio (A_{inlet}/A_9) of 0.63. The short flap nozzle data were acquired at a 17 degree clamshell angle and an ejector inlet area ratio of 0.46. A comparison of data shows that the performance of both subsonic cruise configurations tend to increase with decreasing pressure split. The trend of increasing performance with increasing fan nozzle pressure ratio indicates that the nozzle flow is greatly overexpanded at lower pressure ratios. The higher performance associated with decreased pressure split is a result of the increased primary flow tending to reduce the overexpansion losses.

The effect of variations in ejector clamshell angle on nozzle performance at subsonic cruise conditions is shown in Figure 5.1-8. The data trends for both configurations indicate that nozzle performance is relatively insensitive to clamshell angle over the range tested. The maximum performance for both configurations occurred over a range of angles from 17 to 21 degrees. The iris configuration exhibited a gross thrust coefficient of 0.878, 1.3 percent higher performance than the short flap nozzle. Additional tests of the iris nozzle, with the clamshell removed, indicated a modest increase in performance, to a gross thrust coefficient of 0.881. Similar tests of the short flap configuration showed a 1 percent improvement in performance.

The effect of variations in ejector inlet area on nozzle performance at subsonic cruise conditions is shown in Figure 5.1-9. The short flap nozzle data were acquired with the clamshell set at 17 degrees. The iris configuration data were obtained with the clamshell removed. Figure 5.1-9 shows that varying the inlet area produced little improvement in the performance of these configurations, i.e., reduction in over expansion or base drag losses by ventilating the ejector shroud. The iris nozzle demonstrated a maximum gross thrust coefficient of 0.881, while a level of 0.865 was attained for the short flap configuration.

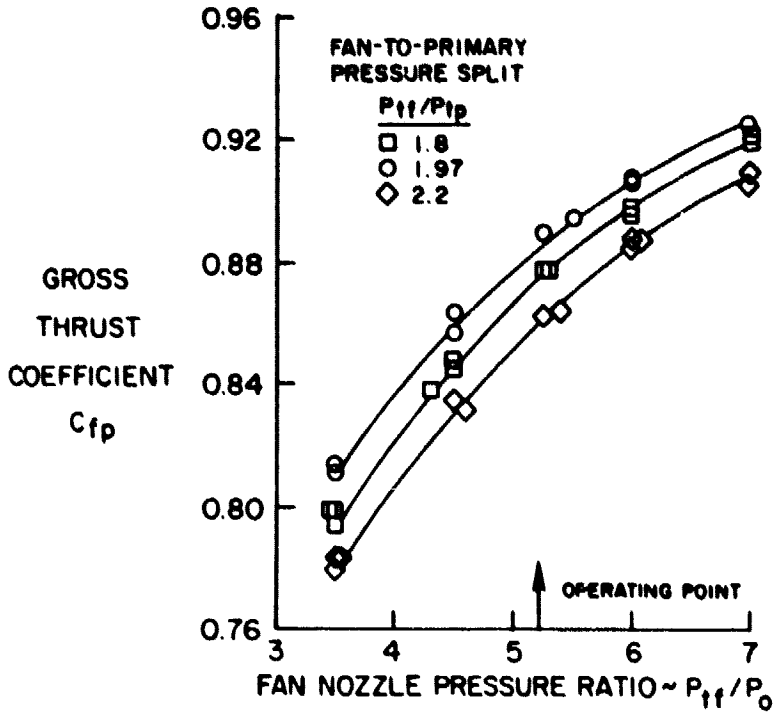

(a) IRIS NOZZLE. CLAMSHELL ANGLE, τ, 21°, EJECTOR INLET-TO-EXIT AREA RATIO, A_{inlet}/A_9, 0.63.

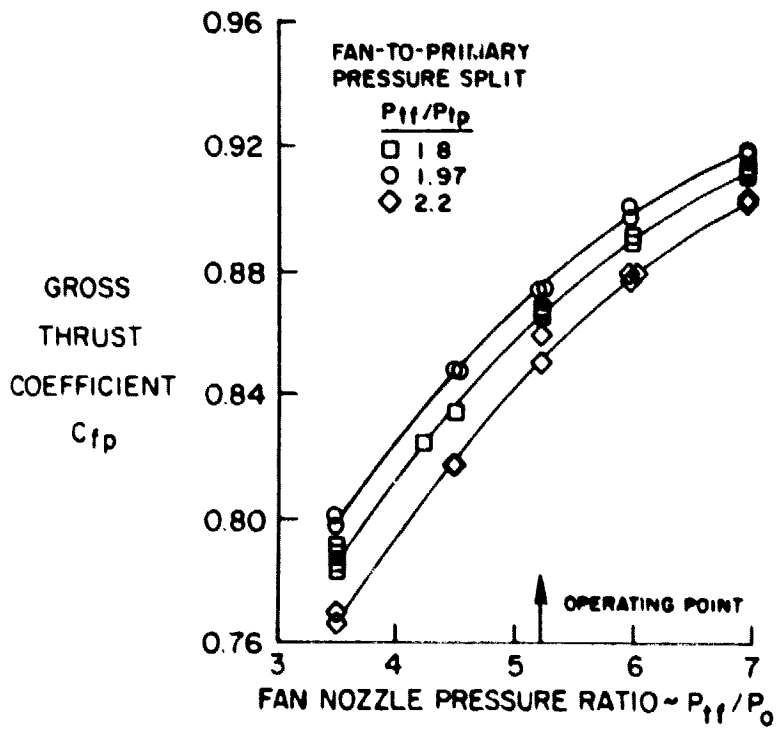

(b) SHORT FLAP NOZZLE. CLAMSHELL ANGLE, τ, 17°, EJECTOR INLET-TO-EXIT AREA RATIO, A_{inlet}/A_9, 0.46

Figure 5.1-7 Comparison of Subsonic Cruise Performance for Various Fan-to-Primary Pressure Splits. Conditions: Free Stream Mach Number, (M_o) 0.9.

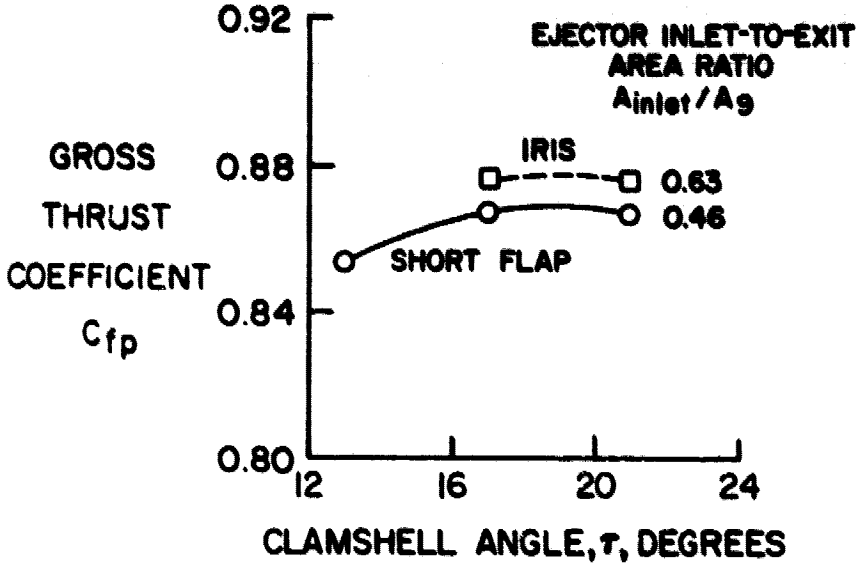

Figure 5.1-8 *Subsonic Performance Sensitivity to Clamshell Angle. Conditions: Free Stream Mach Number, (M_O) 0.9; Fan Nozzle Pressure Ratio, P_{tf}/P_O, 5.26; Fan-to-Primary Pressure Split, P_{tf}/P_{tp}, 1.97.*

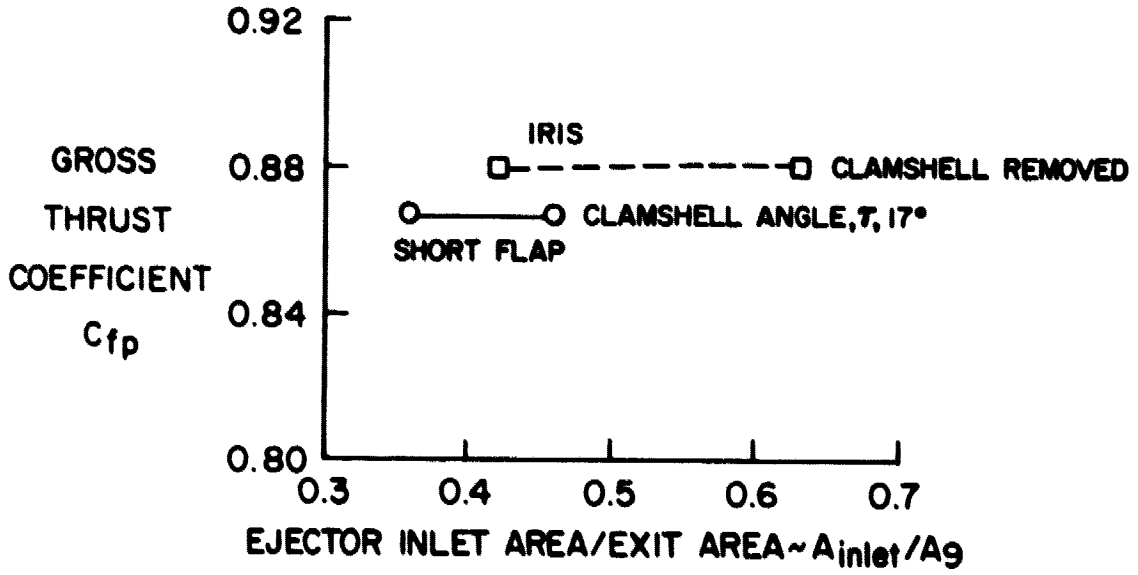

Figure 5.1-8 *Subsonic Performance Sensitivity to Clamshell Angle. Conditions: Free Stream Mach Number, (M_O) 0.9; Fan Nozzle Pressure Ratio, P_{tf}/P_O, 5.26; Fan-to-Primary Pressure Split, P_{tf}/P_{tp}, 1.97.*

The measured subsonic performance, as presented in Figures 5.1-7 through 5.1-9, was lower than expected. Diagnostic tests were conducted to understand these deficiencies. Emphasis was placed on the iris configuration because of its higher performance level. Both configurations were tested over a range of Mach numbers to determine the effects of external flow on performance, as shown in Figure 5.1-10. The data show that performance deficiencies are related to external flow effects since both nozzles demonstrated significantly higher performance levels at static conditions; the iris configuration showing the highest potential at a level of 0.975.

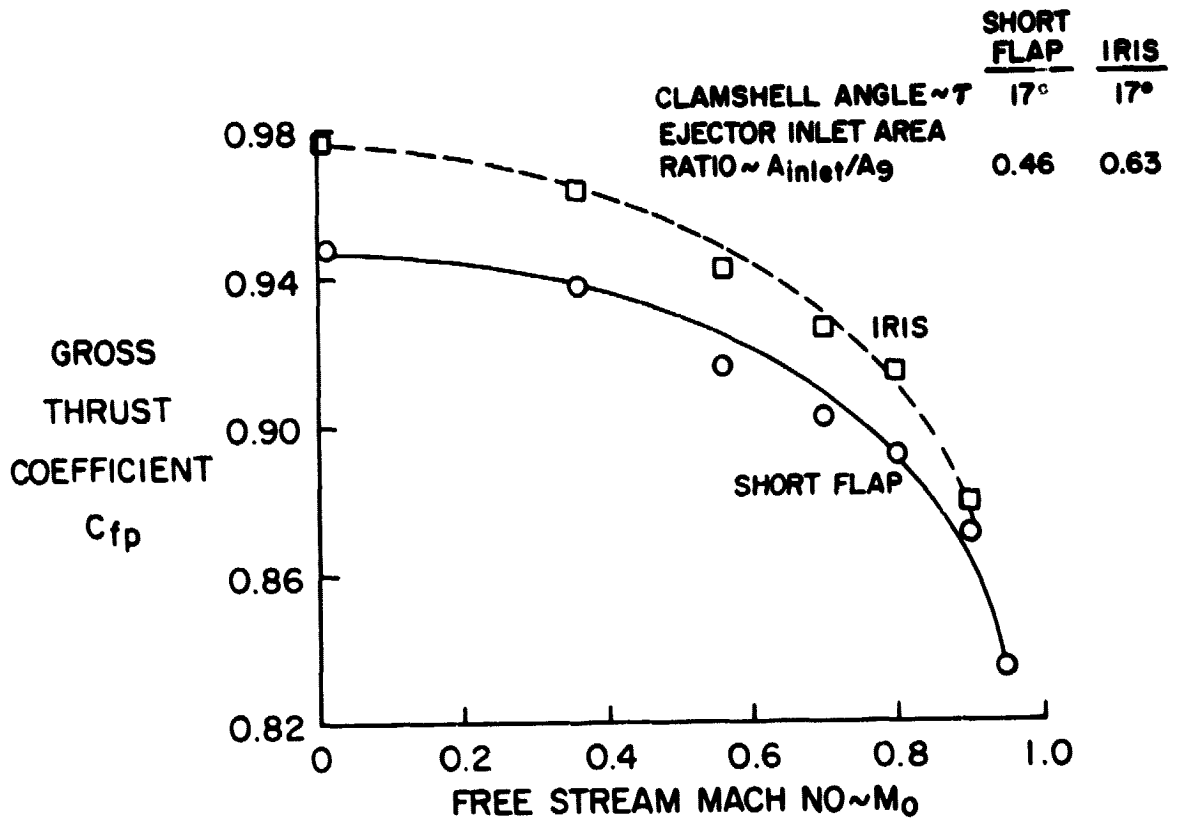

Figure 5.1-10 Effect of Free Stream Mach Number on Subsonic Cruise Nozzle Performance. Conditions: Fan Nozzle Pressure Ratio, P_{tf}/P_o, 5.26; Fan-to-Primary Pressure Split, P_{tf}/P_{tp}, 1.97.

The iris configuration was also tested over a range of free stream Mach numbers with the ejector shroud removed. A comparison of these results to data with the shroud in place (Figure 5.1.11a) shows a very similar performance trend as a function of free stream Mach number. The results imply that boattail drag of the ejector inlet base is the problem. An integration of the static pressure distribution over the boattail at Mach number of 0.9, shown in Figure 5.1-11b, confirms this observation. The integrated boattail drag in terms of incremental gross thrust coefficient is a large part of the performance difference between static and 0.9 free stream Mach number test conditions.

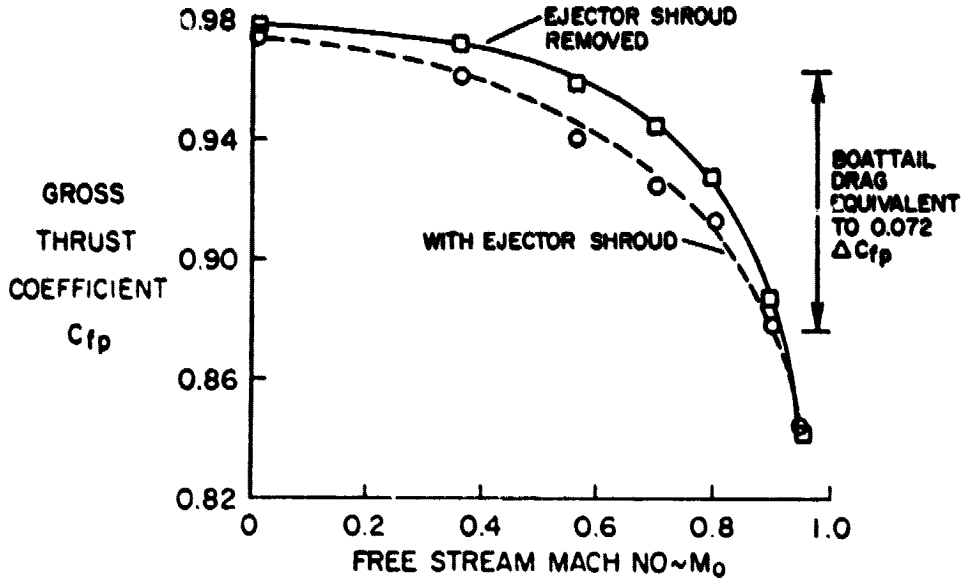

(a) COMPARISON OF NOZZLE PERFORMANCE WITH AND WITHOUT EJECTOR SHROUD.

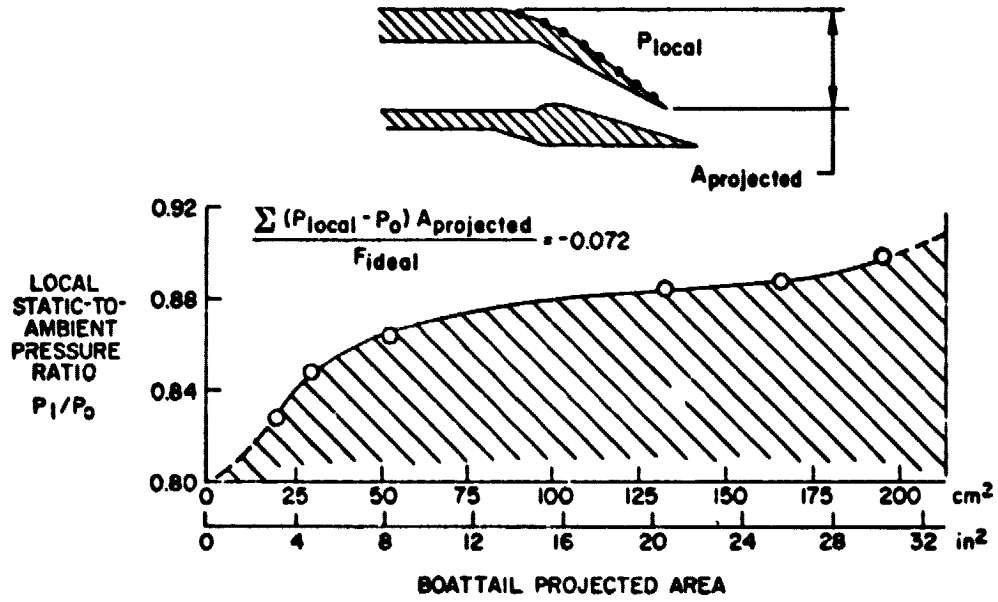

(b) PRESSURE DRAG ON IRIS NOZZLE BOATTAIL RELATED TO SUBSONIC CRUISE THRUST LOSS, EJECTOR REMOVED, M_0=0.9

Figure 5.1-11 Influence of Mach Number on Iris Nozzle Performance With and Without Shroud. Conditions: Mach Number, (M_0), 0.9 Fan Nozzle Pressure Ratio, P_{tf}/P_0, 5.26; Fan-to-Primary Pressure Split, P_{tf}/P_{tp}, 1.97.

5.1.3 Takeoff Performance

The takeoff configuration of the short flap nozzle was tested over a range of clamshell positions and ejector inlet areas at static and 0.36 free stream Mach number conditions to determine the optimum geometry of the ejector shroud components. The influence of clamshell position on nozzle performance at the takeoff condition is shown in Figure 5.1-12. Data trends are similar at both the static and 0.36 Mach number conditions, and show that the minimum clamshell angle tested, 13 degrees, results in the highest performance. The effect of ejector inlet area on takeoff performance is presented in Figure 5.1-13. The data show that the performance of these configurations is relatively insensitive to inlet area variation over the range tested. A comparison of the data also shows a decrease in performance from static conditions to 0.36 M_o. The performance decrease with free stream flow indicates a lack of tertiary flow through the ejector inlet to ventilate the shroud.

The iris takeoff configuration was tested with the clamshell positioned at 13 degrees (τ) and the inlet area (A_{inlet}/A_9) set at 0.80. The results are compared to the best performing short flap configuration τ of 13° and A_{inlet}/A_9 of 0.46 in Figures 5.1-14a and b at static and 0.36 Mach number conditions. As indicated, the performance of the iris confiquration is superior to the short flap over the range of fan nozzle pressure ratio tested. At takeoff conditions, the static performance of the iris nozzle is 0.980, 4 percent higher than the short flap. At a Mach number of 0.36, iris nozzle performance decreases to 0.966, but still provides a 4 percent advantage over the short flap configuration.

A comparison of data at the two fan to primary pressure ratios tested, 1.46 and 1.7, is shown in Figure 5.1-15. Results show that performance of the takeoff configurations is insensitive to pressure split.

Primary nozzle operating conditions at supersonic and subsonic cruise require a convergent-divergent nozzle design for optimum performance. At takeoff, operating conditions are below sonic requiring a convergent flowpath to minimize overexpansion performance losses. These diverse flowpath requirements are satisfied by the split translating centerbody plug, but with an added degree of mechanical complexity over a solid type plug nozzle as shown in Figure 3.2-4c.

To evaluate the performance benefits of a split plug design, the takeoff configurations were tested with the plug retracted. A comparison of nozzle performance with the split plug retracted and extended is presented in Figure 5.1-16. The comparison shows that the complexity of the split plug design is warranted to obtain maximum takeoff performance. With the plug retracted, the iris nozzle loses 2.5 percent in static performance and 2 percent at 0.36 Mach number. This loss is a direct result of the flow being overexpanded in the primary nozzle. The short flap configuration exhibited a similar performance loss at the 0.36 Mach number condition.

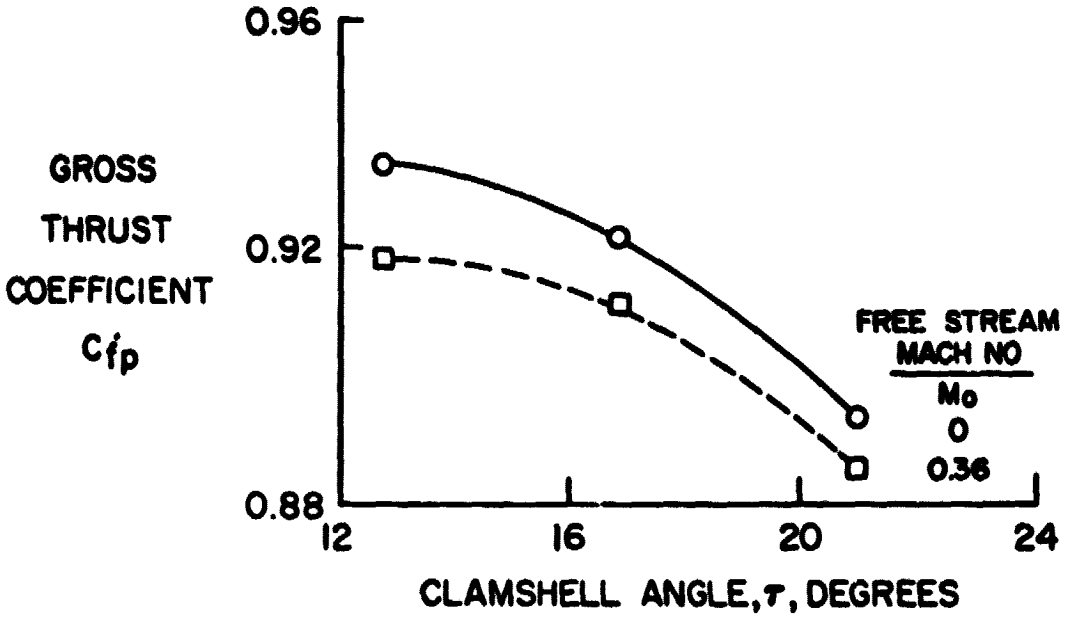

Figure 5.1-12 Influence of Clamshell Position on Short Flap Nozzle Performance. Conditions: Fan Nozzle Pressure Ratio, P_{tf}/P_o, 2.5; Fan-to-Primary Pressure Split, P_{tf}/P_o, 1.46; Ejector Inlet Area Ratio, A_{inlet}/A_9, 0.46.

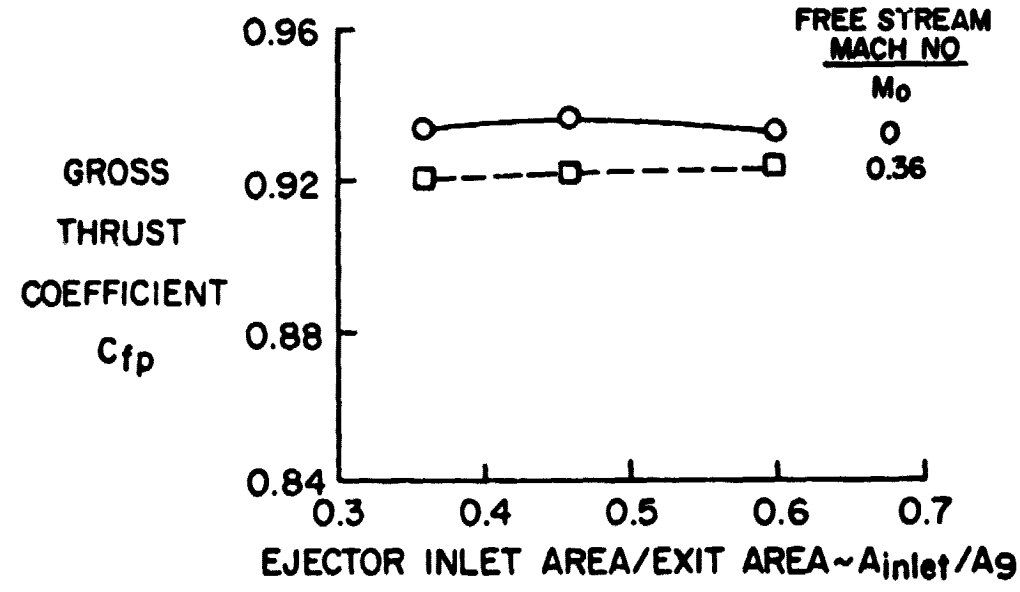

Figure 5.1-13 Influence of Ejector Inlet Area on Short Flap Nozzle Performance. Conditions: Fan Nozzle Pressure Ratio, P_{tf}/P_o, 1.46; Fan-to-Primary Pressure Split, P_{tf}/P_o, 1.46; Clamshell Angle, τ, 13°.

Analysis of the short flap takeoff performance as a function of P_{ft}/P_o, previously illustrated in Figure 5.1-14, shows that lowest measured performance occurs at takeoff engine operating conditions. The performance decrease is attributed to overexpansion of the fan flow on the isentropic splitter. A plot of the limited static pressures on the splitter, Figure 5.1-17, indicates an initial region of overexpanded flow downstream of the nozzle throat. Exploratory tests were conducted to determine the cause of these losses. It was found that the overexpansion losses were influenced by two design elements: (1) the close proximity of the ejector inlet flap to the fan nozzle lip created a convergent-divergent nozzle effect and (2) the fan nozzle-splitter shape.

Tests of the short flap configuration with the 20-degree trailing edge portion of the ejector inlet flap removed, showed a 1.5 percent improvement in performance, as illustrated in Figure 5.1-18. However, the trend still indicates an overexpansion characteristic at takeoff engine operating conditions. A comparison of the static pressure distributions of the original and modified configurations (Figure 5.1-19) shows that the modification reduced the initial overexpansion region, but did not completely eliminate the loss. Examination of the geometry of the fan nozzle flap relative to the crown of the flow splitter indicated that the throat flow may be underturned, which would explain the residual overexpansion loss. Increased flow turning can be obtained by revising the kinematics of the nozzle flap mechanism to relocate the flap lip in the takeoff mode.

Exploratory tests of the iris takeoff configuration were conducted to investigate the fall-off in performance with increasing fan nozzle pressure ratio. This included testing with the ejector clamshell removed. The test revealed that the exhaust flow was impinging on the clamshell. A comparison of iris nozzle performance with and without the clamshell is presented in Figure 5.1-20. The comparison shows that removal of the clamshell decreased the performance fall-off with increasing pressure ratio. The data show that if the clamshell impingement could be avoided, the iris configuration could achieve takeoff performance comparable to the levels assumed in the Advanced Supersonic Transport studies. One way to avoid impingement of the nozzle jet plume on the clamshell, would be a reduction in fan nozzle radius ratio to reduce the plume diameter.

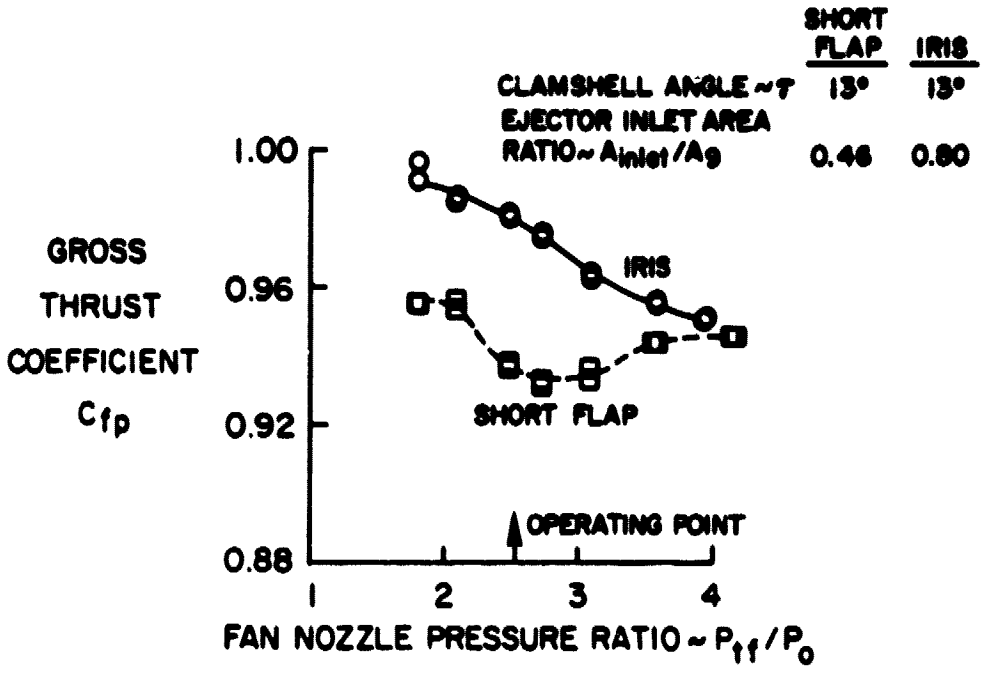

(a) FREE STREAM MACH NUMBER, M_0, 0.

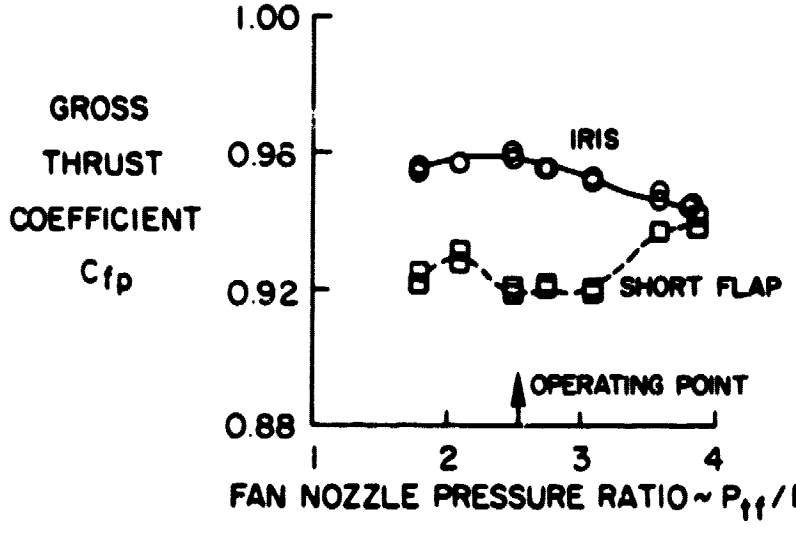

(b) FREE STREAM MACH NUMBER, M_0, 0.36

Figure 5.1-14 Performance Comparison of Iris and Short Flap Takeoff Configurations. Condition: Fan-to-Primary Pressure Split, P_{tf}/P_{tp}, 1.46.

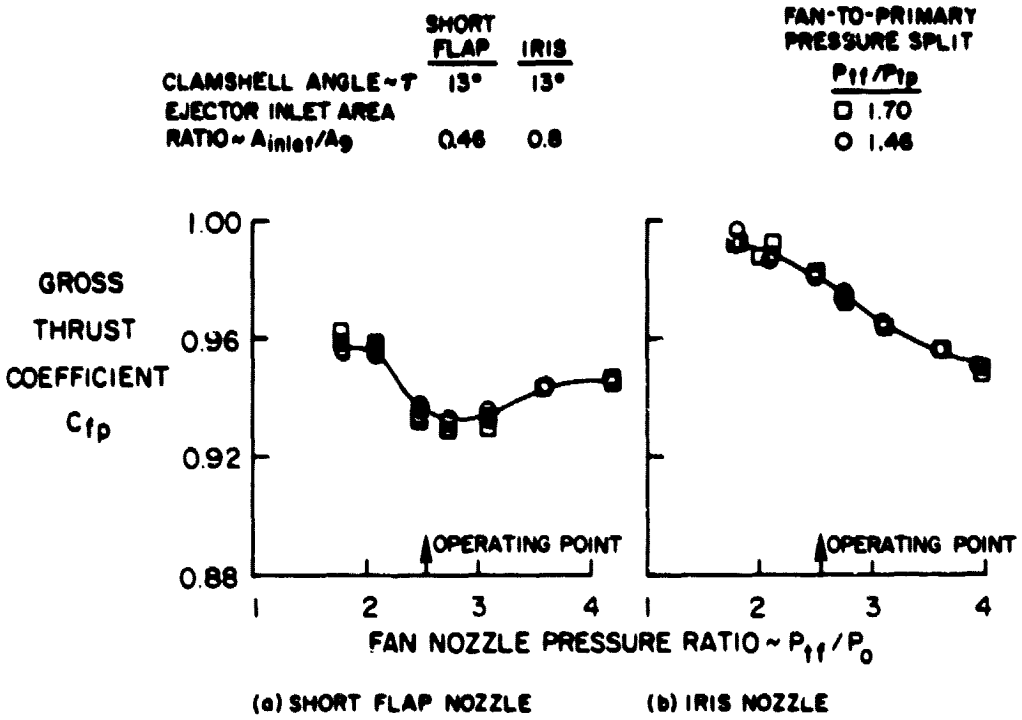

Figure 5.1-15 Effect of Fan-to Primary Pressure Split on Nozzle Performance. Conditions: Free Stream Mach Number, (M_o), 0.

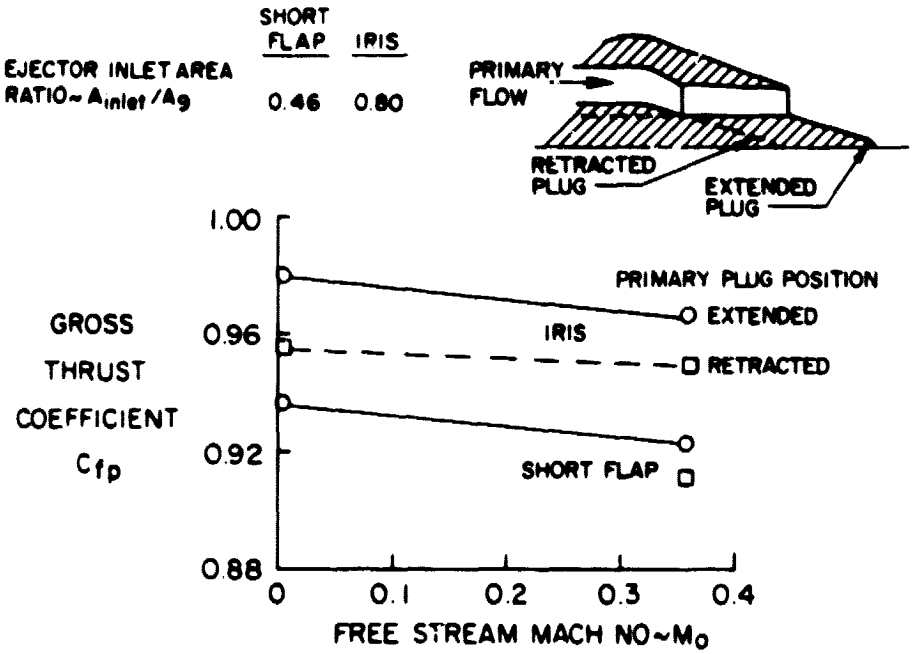

Figure 5.1-16 Comparison of Takeoff Nozzle Performance with Primary Plug Extended and Retracted. Conditions: Fan Nozzle Pressure Ratio, P_{tf}/P_o, 2.5; Fan-to-Primary Pressure Split, P_{tf}/P_{tp}, 1.46; Clamshell Angle, τ, 13°.

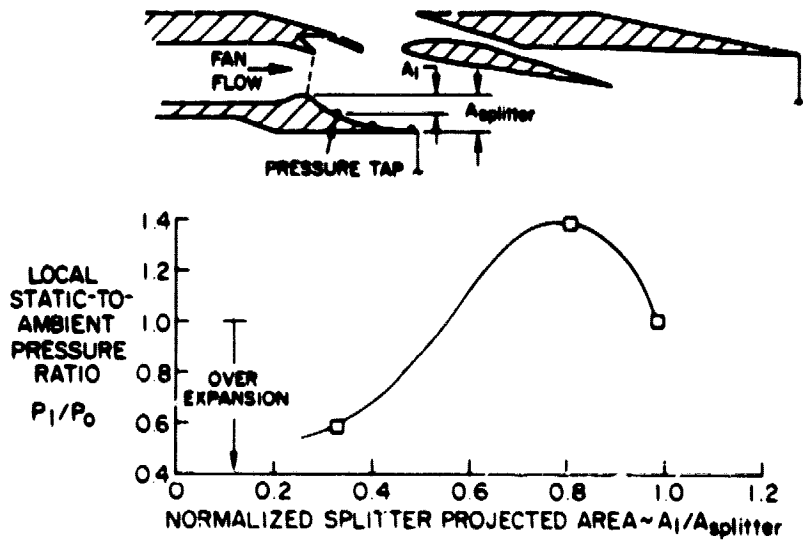

Figure 5.1-17 Short Flap Nozzle Splitter Static Pressure Distribution. Conditions: Fan Nozzle Pressure Ratio, P_{tf}/P_o, 2.5; Fan-to-Primary Pressure Split, P_{tf}/P_{tp}, 1.46; Clamshell Angle, τ, 13°; Ejector Inlet Area, A_{inlet}/A_9, 0.46; Free Stream Mach Number, (M_o), 0.

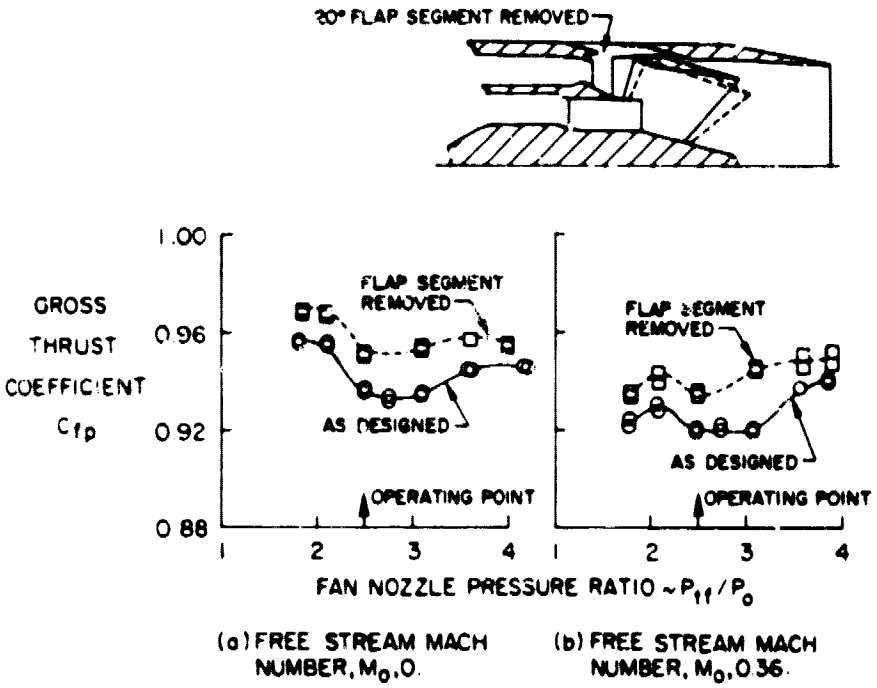

Figure 5.1-18 Comparison of Original and Modified Short Flap Nozzle Takeoff Performance. Conditions: Fan-to-Primary Pressure Split, P_{tf}/P_{tp}, 1.46; Clamshell Angle, τ, 13°; Ejector Inlet Area, A_{inlet}/A_9, 0.46.

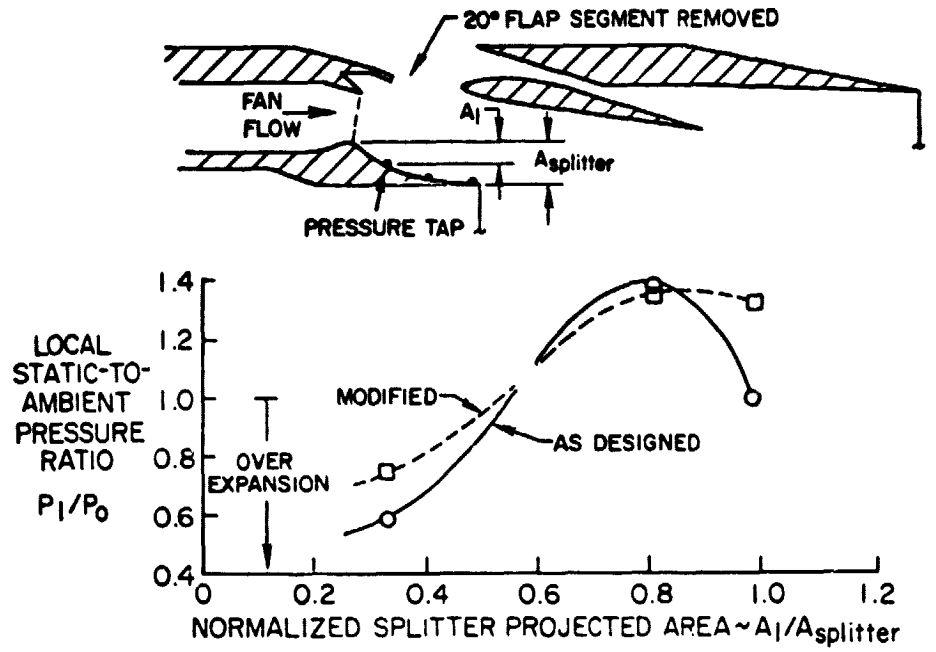

Figure 5.1-19 Comparison of Original and Modified Short Flap Nozzle Splitter Static Pressure Distributions. Conditions: Fan-to-Primary Pressure Split, P_{tf}/P_{tp}, 1.46; Clamshell Angle, τ, 13°; Ejector Inlet Area, A_{inlet}/A_9, 0.46; Free Stream Mach Number, (M_o), 0.

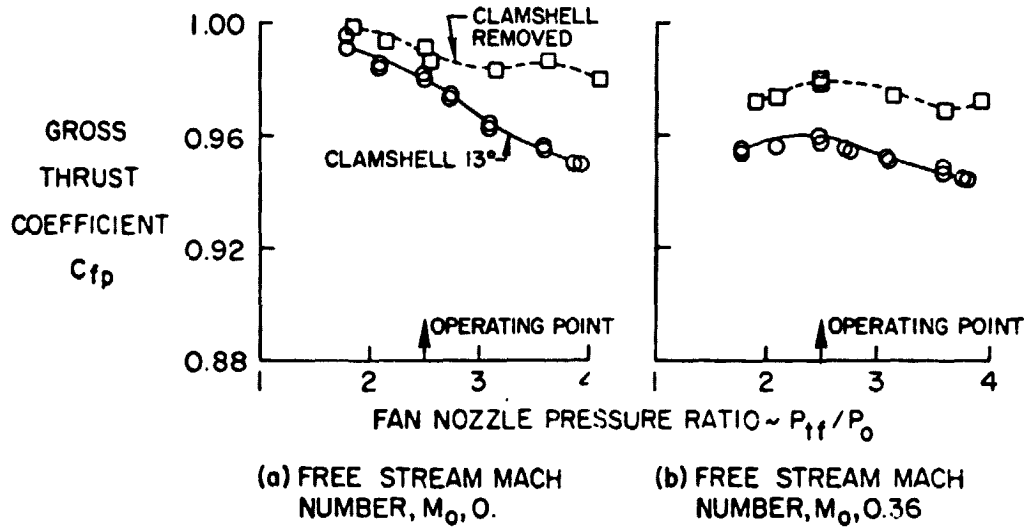

Figure 5.1-20 Comparison of Iris Nozzle Takeoff Performance With and Without Ejector Clamshell. Conditions: Fan-to-Primary Pressure Split, P_{tf}/P_{tp}, 1.46; Ejector Inlet Area, A_{inlet}/A_9, 0.8

5.1.4 Comparison of Results with Advanced Supersonic Transport Propulsion Study Performance Levels

A comparison of the measured nozzle performance to levels assumed in the Advanced Supersonic Transport propulsion studies (refer to Table 3.2-II) is illustrated in Figure 5.1-21. Data are shown for both the iris and short flap configurations at simulated engine operating conditions and flight Mach numbers. The comparison shows that at supersonic cruise the performance of both configurations at zero secondary flow achieved the Advanced Supersonic Transport study level, the iris and short flap configurations demonstrating gross thrust coefficients of 0.980 and 0.984, respectively. To date, integrated propulsion studies have not been conducted in sufficient depth to evaluate the overall benefit of secondary flow. The comparison also shows that at subsonic cruise the performance of both configurations is deficient, 6 percent for the iris and 7.5 percent for the short flap configuration. At takeoff conditions, the performance of the iris configuration approached the study levels within 0.5 percent statically but was 2 percent lower at climbout. The short flap configuration, however, was deficient by 4 to 6 percent.

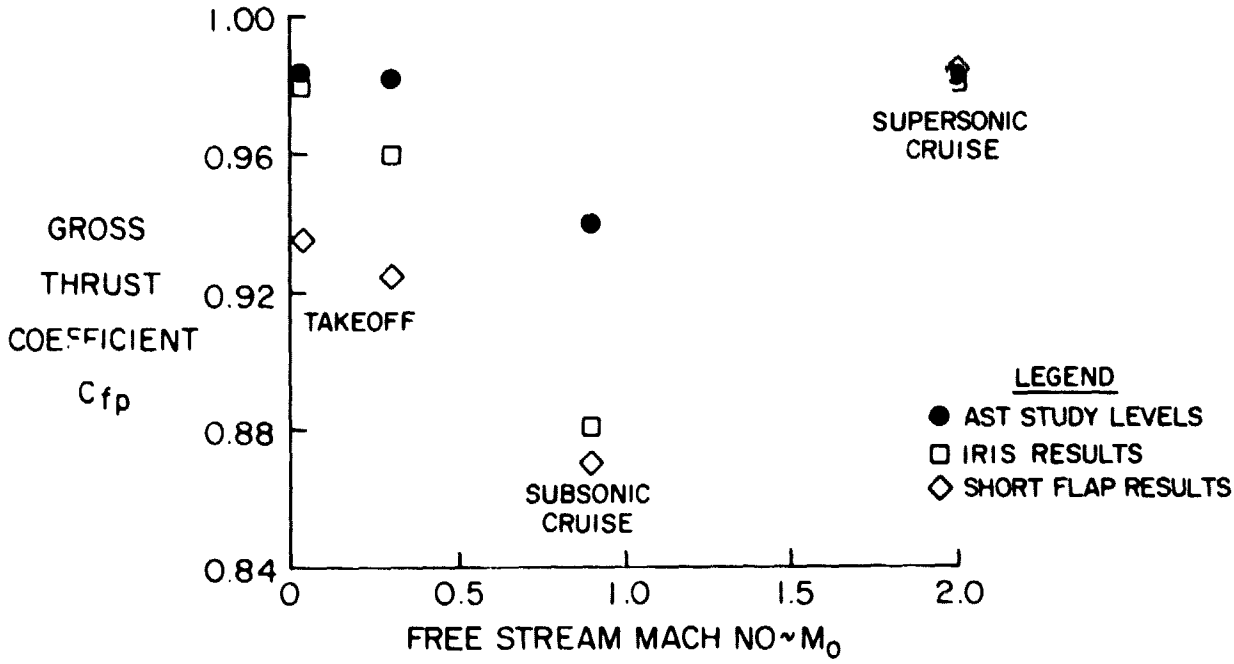

Figure 5.1-21 Comparison of Test Results with AST Propulsion Study Nozzle Performance. Condition: Corrected Secondary Flow, $W_{S\ corr}$, 0%.

5.2 NOZZLE DISCHARGE COEFFICIENTS

5.2.1 Supersonic Cruise Configuration Discharge Coefficients

Fan and primary nozzle discharge coefficients (C_{D_f} and C_{D_p}, respectively) for the iris and short flap supersonic cruise configurations are presented in Figure 5.2-1. Data are presented for the extreme range of conditions tested; fan to primary pressure split of 2.0 and 2.6 and corrected secondary flow of zero and 4 percent. The data collapse shows that both the fan and primary discharge coefficients are almost independent of nozzle operating conditions and corrected secondary flow. At nozzle operating conditions well above the critical flow regime, the trend of the data is nearly constant with nozzle pressure ratio. At engine operating conditions, the levels of fan and primary discharge coefficients for the iris configuration are 0.962 and 0.991, respectively. Levels exhibited by the short flap configuration are a fan discharge coefficient of 0.975 and a primary nozzle discharge coefficient of 0.982.

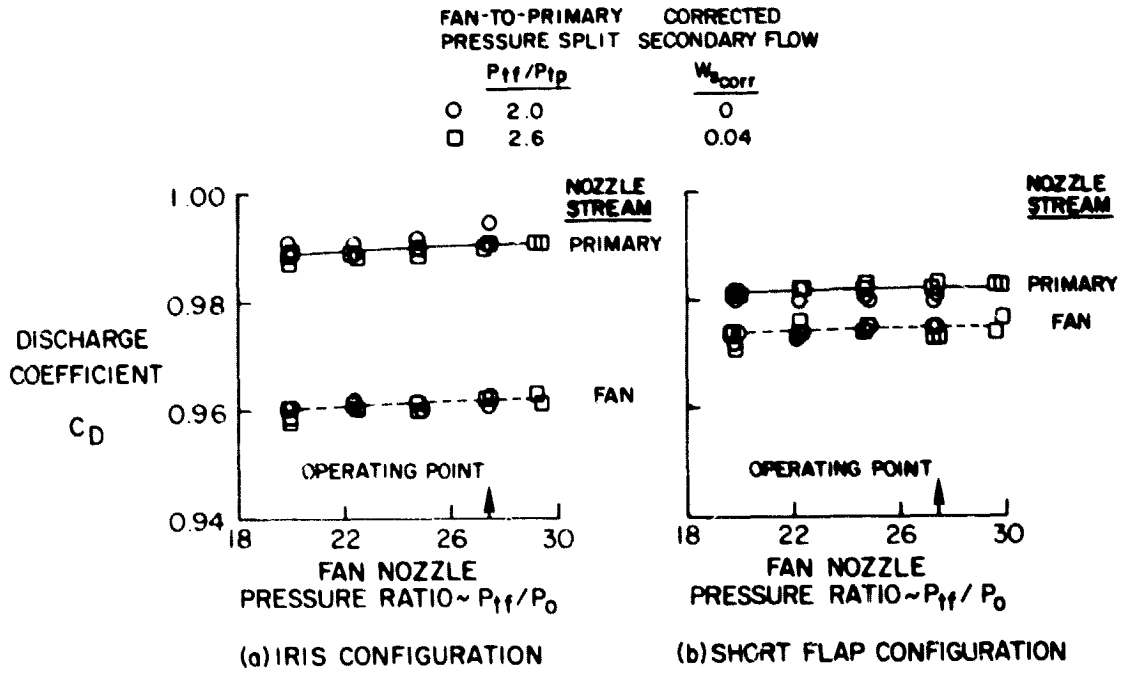

Figure 5.2-1 *Iris and Short Flap Supersonic Cruise Configuration Discharge Coefficients. Conditions: Free Stream Mach Number, (M_o), 2.0.*

5.2.2 Subsonic Cruise Configuration Discharge Coefficients

Figure 5.2-2 presents fan and primary discharge coefficients for the iris and short flap subsonic cruise configurations. For each plot, data are presented for the three fan to primary pressure splits tested. The collapse of fan nozzle data to a constant value again shows that the fan discharge coefficient is independent of nozzle operating conditions over the range tested. A similar collapse is observed for primary nozzle data at pressure splits of 1.8 and 1.97. However, at a fan to primary pressure split of 2.2, the primary nozzle discharge coefficient increases to values near 1.0 at a fan pressure ratio of 3.5 for both configurations. The corresponding primary pressure ratio for these conditions is 1.6, which is in the unchoked subsonic flow regime. At subcritical nozzle flow conditions, there are two possible reasons for the increased discharge coefficients: (1) fan flow was aspirating the primary flow or (2) the characteristic of a convergent-divergent nozzle to produce discharge coefficients greater than unity due to overexpansion of the flow. At engine operating conditions, the levels of fan and primary discharge coefficients for the iris configuration are 0.960 and 0.985, respectively. Levels observed for the short flap configuration are a fan discharge coefficient of 0.967 and a primary nozzle discharge coefficient of 0.981.

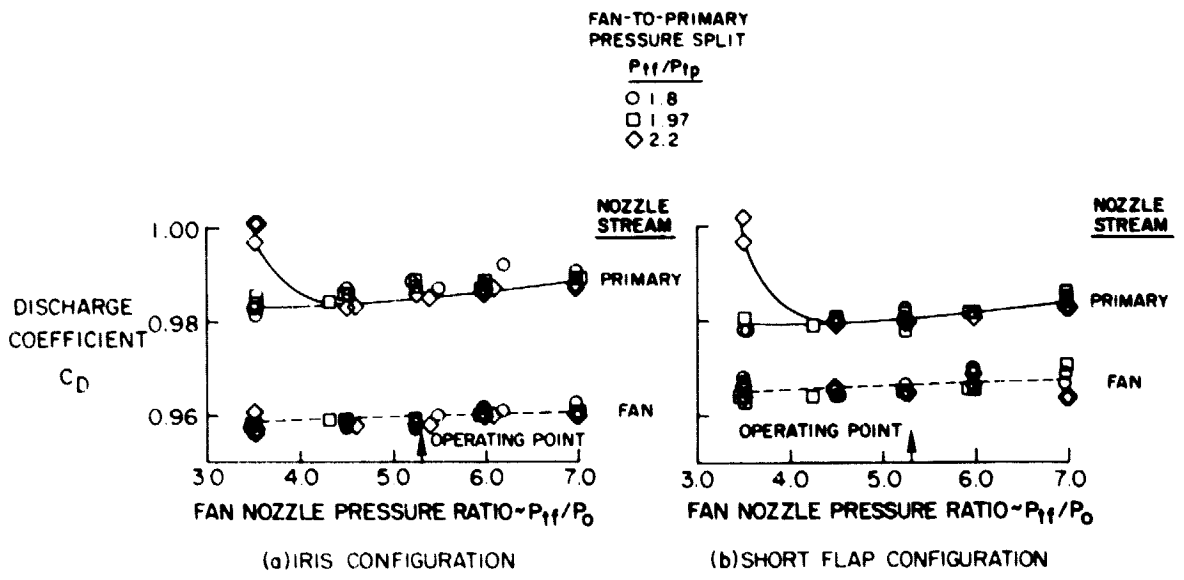

Figure 5.2-2 Iris and Short Flap Subsonic Cruise Configuration Discharge Coefficients. Conditons: Free Stream Mach Number, (M_0), 0.9.

5.2.3 Takeoff Configuration Discharge Coefficients

Fan and primary nozzle discharge coefficients for the iris takeoff configuration are illustrated in Figure 5.2-3. Data are presented for both pressure splits tested at static and 0.36 free stream Mach number conditions. As observed previously, fan nozzle data for all test conditions collapsed to a single curve. The data exhibit a conventional trend with decreasing fan nozzle pressure ratio, tending to decrease slightly near sonic flow conditions. Trends of primary nozzle discharge coefficients, on the other hand, indicate that the primary nozzle discharge coefficient is a function of fan to primary pressure split and free stream flow conditions. The figures also show that the data are not monotonic as a function of primary pressure ratio. The external flow interaction is very strong at low pressure ratios (e.g., 1.1) decreasing the discharge coefficient by 5 to 12 percent relative to the levels observed statically. However, in the range of takeoff operating conditions, the variation of primary nozzle discharge coefficient is approximately 2 percent. Measured values of fan and primary discharge coefficients at both static and 0.36 M_o conditions are 0.950 and 0.960, respectively.

Discharge coefficient data for the short flap takeoff configuration are presented in Figure 5.2-4. The characteristics of the fan nozzle data are consistent with that observed previously. The trend of the primary nozzle discharge coefficient, increasing to values greater than unity in the unchoked flow regime, indicates that the fan flow over the isentropic splitter is aspirating the primary flow. Data at both pressure splits collapsed to a single curve as a function of primary nozzle pressure ratio, illustrating that the primary nozzle discharge coefficient is independent of the fan to primary pressure split. At engine operating conditions, the levels of fan and primary discharge coefficients for the short flap configuration are 0.968 and 0.980, respectively, for the two free stream conditions tested.

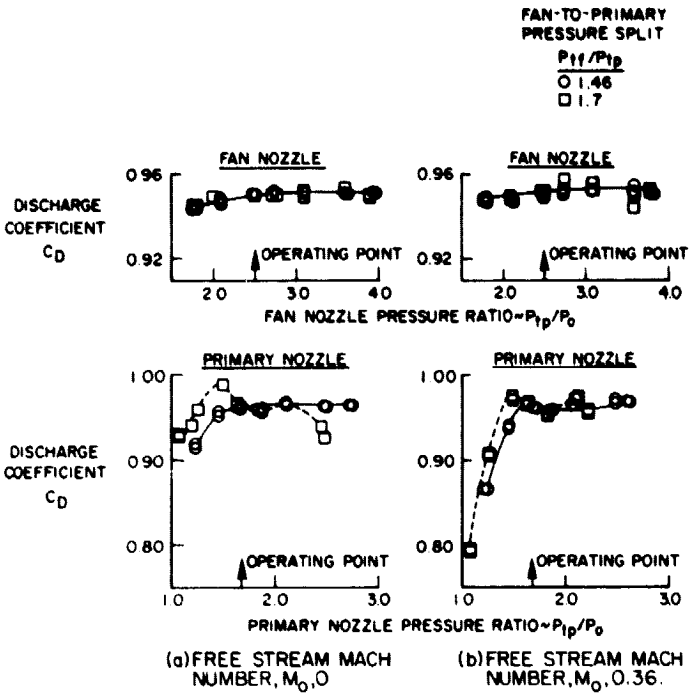

Figure 5.2-3 Iris Takeoff Configuration Discharge Coefficients.

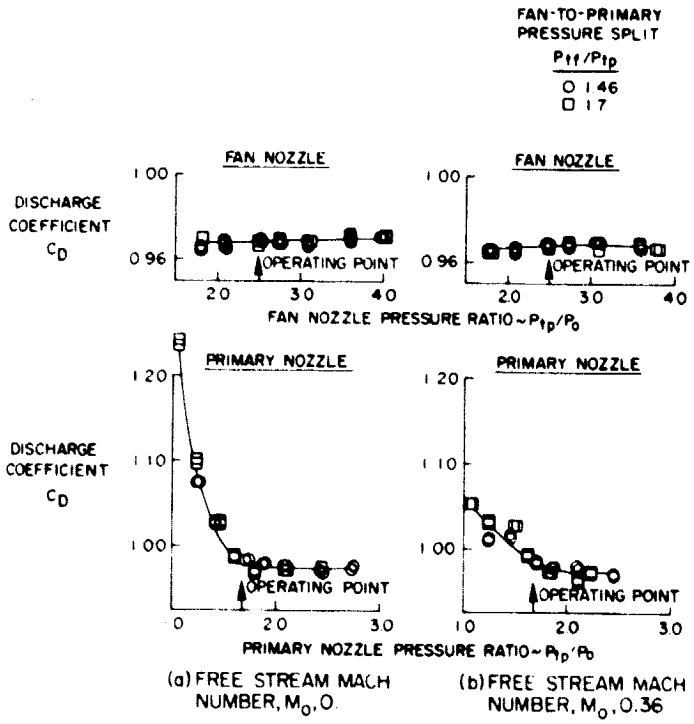

Figure 5.2-4 Short Flap Takeoff Configuration Discharge Coefficients.

SECTION 6.0

CONCLUSIONS

The performance of two variable geometry coannular ejector nozzle models for an Advanced Supersonic Transport was obtained at key supersonic and subsonic flight conditions over a range of engine operating conditions. The significant results of the tests are summarized below.

Supersonic Cruise Results

Both configurations demonstrated good supersonic cruise performance comparable to the level assumed in the Advanced Supersonic Transport propulsion studies, a gross thrust coefficient of 0.982, at zero secondary flow. The addition of 2 and 4 percent secondary flow increased iris nozzle performance by 2.6 and 4.1 percent, respectively, while short flap nozzle performance increased 2.3 and 3.5 percent. Variation of fan to primary pressure split had no effect on nozzle performance over the range tested.

Subsonic Cruise Results

The performance of both subsonic cruise configurations was deficient relative to the Advanced Supersonic Transport study gross thrust level of 0.94. The iris configuration fell short of the target by 6 percent and the short flap was deficient by 7.5 percent. Exploratory tests showed the performance deficiencies resulted from inadequate ventilation of the ejector shroud which resulted in excessive ejector inlet boattail drag. Mission emphasis on supersonic performance established nozzle length requirements and constrained the ejector inlet design. Variation of ejector inlet area and clamshell position had minimal effect on nozzle performance for the range tested.

Takeoff Results

Performance of the iris takeoff configuration approached the Advanced Supersonic Transport study levels at static conditions but was 2 percent low at climbout. The short flap configuration was deficient by 4 and 6 percent at these conditions. Exploratory tests of the iris configuration showed that flow impingement on the ejector clamshell degraded the performance 0.5 to 2 percent. Additional tests of the short flap configuration showed that modifications of the ejector inlet flap would provide limited performance improvements.

REFERENCES

1. Howlett, R. A., et.al., "Advanced Supersonic Propulsion Study," NASA CR-135184, 1976.

2. Kozlowski, H., and Packman, A. B., "Aero/Acoustic Tests of Duct Burning Turbofan Nozzles," NASA CR-2628, 1976.

3. Kozlowski, H., and Packman, A. B., "Flight Effects of the Aero/ Acoustic Characteristics of Inverted Velocity Profile Coannular Nozzles," NASA CR-3018, 1978.

4. Larson, R. S., Nelson, D. P., and Stevens, B. S., "Aerodynamic and Acoustic Investigation of Inverted Velocity Profile Coannular Exhaust Nozzle Models and Development of Aerodynamic and Acoustic Prediction Procedures," NASA CR-3168, 1979.

5. Nelson, D. P., "Model Aerodynamic Test Results for Two Variable Cycle Engine Coannular Exhaust Systems at Takeoff and Cruise Conditions - Comprehensive Data Report," NASA CR-159819, 1981.

6. Swallow, Robert J., and Aiello, Robert A., "NASA Lewis 8 by 6 Foot Supersonic Wind Tunnel," NASA TM X-71542, May, 1974.

7. Staid, Paul S., "Wind Tunnel Performance Tests of Coannular Plug Nozzles," NASA CR 2990, 1978.

8. Johnson, R. C., "Real-Gas Effects in Critical Flow Through Nozzles and Tabulated Thermodynamic Properties," NASA TN D-2565, 1965.

9. Smith, K. D., "Methods and Charts for Estimating Skin Friction Drag in Wind Tunnel Tests with Zero Heat Transfer," C.P. No. 824, Great Britain, 1965.

APPENDIX A

FACILITY VERIFICATION

A modified Supersonic Tunnel Association nozzle was constructed for this program and tested as a means of verifying the force and weight-flow measurement accuracy of the facility. The procedure and results are discussed in this Appendix.

Calibration Model Description

The geometric details of the modified Supersonic Tunnel Association nozzle are shown in Figure A-1. This nozzle is essentially an American Society of Mechanical Engineers standard nozzle with a base. The modified Supersonic Tunnel Association nozzle, installed in the wind tunnel, is shown in Figure A-2. Testing with this nozzle was conducted with either the fan flow (W_f) or primary flow (W_p), but never with both flows simultaneously. Flow conditioning was provided by means of perforated "choke" plates and screens upstream of the nozzle. Nozzle total pressure was measured by two four-tube rakes, while nozzle total temperature was measured with two copper constantan thermocouples. Base static pressure was determined using four rows of six taps.

Calibration Model Data Reduction

In order to compare the modified Supersonic Tunnel Association nozzle thrust coefficients with semi-empirical predicted levels, it was necessary to modify the thrust coefficient (C_{f_p}) as defined by Equation 18 to account for the nozzle base drag, D_{ex}:

$$C_{F,int} = \frac{F - D_{ex}}{mV_i} + \frac{D_B}{mV_i} \tag{1A}$$

or

$$C_{F,int} = C_{fp} + \Delta C_{fB} \tag{2A}$$

where C_{f_p} is the nozzle thrust coefficient corrected for friction drag as previously defined, D_B is the nozzle base drag as measured by twenty-four static pressure taps over the base area.

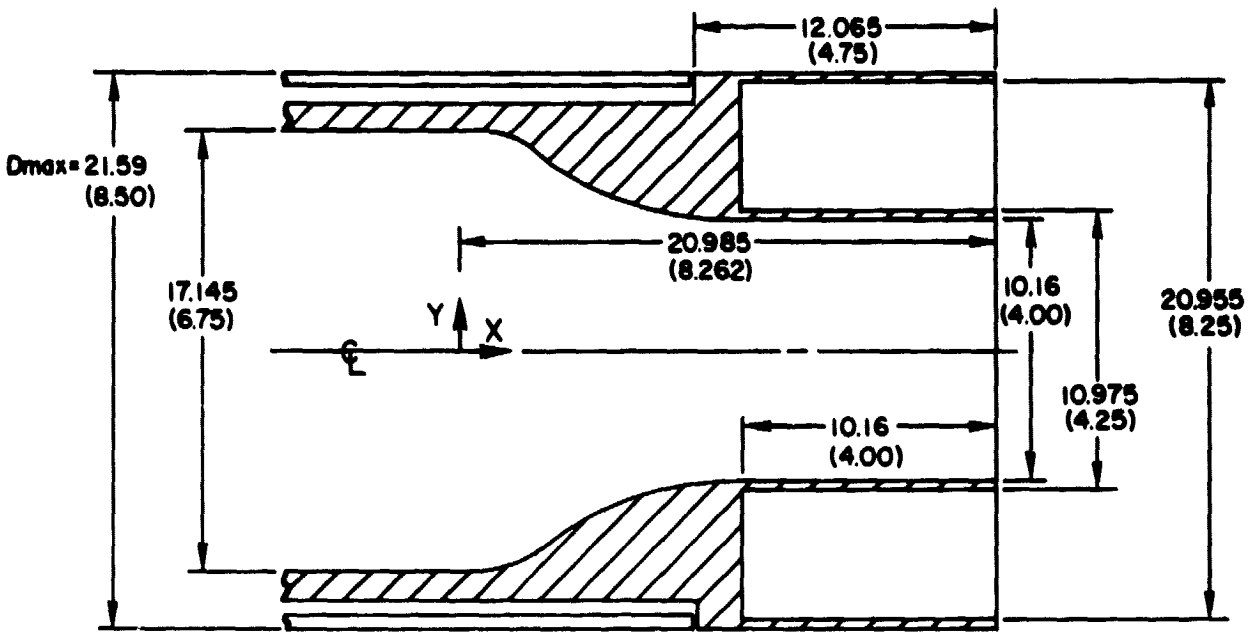

Nozzle Internal Coordinates

X Coordinates		Y Coordinates		
cm	in	cm	in	
0	(0)	8.573	(3.375)	Circular
0.665	(0.262)	8.529	(3.358)	
1.300	(0.512)	8.402	(3.308)	
1.935	(0.752)	8.189	(3.224)	
2.570	(1.012)	7.877	(3.101)	Elliptical
3.205	(1.262)	7.351	(2.894)	
3.840	(1.512)	6.916	(2.723)	
4.479	(1.762)	6.551	(2.579)	
5.110	(2.012)	6.241	(2.457)	
5.745	(2.262)	5.979	(2.354)	
6.380	(2.512)	5.756	(2.266)	
7.015	(2.762)	5.570	(2.193)	
7.650	(3.012)	5.415	(2.132)	
8.285	(3.262)	5.293	(2.084)	
8.920	(3.512)	5.199	(2.047)	
9.555	(3.762)	5.133	(2.021)	
10.190	(4.012)	5.093	(2.005)	
10.825	(4.262)	5.080	(2.000)	Cylindrical
20.985	(8.262)	5.080	(2.000)	

Figure A-1 *Geometric Details of Modified Supersonic Tunnel Association (STA) Nozzle. All Dimensions are in cm (in).*

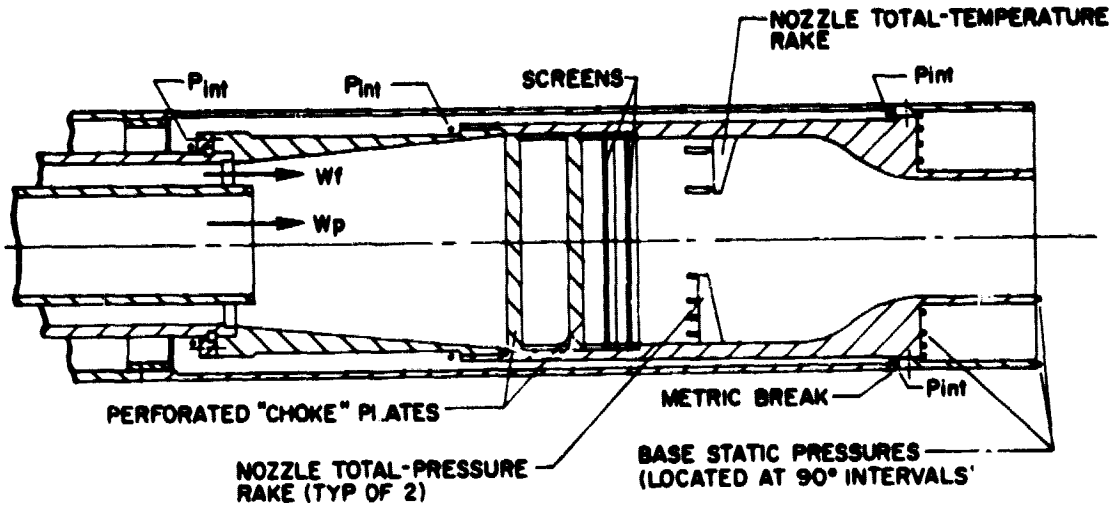

Figure A-2 *Details of Modified Supersonic Tunnel Association Nozzle Installation.*

Calibration Model Results

Internal thrust coefficients for the modified Supersonic Tunnel Association nozzle are presented in Figure A-3. Data were obtained at quiescent conditions and at Mach numbers 0.36, 0.9, and 2.0. Testing was conducted by flowing air from either the fan or primary supply system. The majority of the data shown were obtained using the large fan flow measuring venturi (D_{vf} = 4.4392 cm (1.7477 in)). The predicted levels of internal thrust coefficient were derived from semi-empirical methods of calculating standard American Society of Mechanical Engineers long radius nozzle performance, as described in Reference 7.

The American Society of Mechanical Engineers equations were slightly modified to include the effect of a small difference in length of the internal flowpaths between the American Society of Mechanical Engineers and modified Supersonic Tunnel Association nozzles. Internal thrust coefficients were generally within ±0.5 percent of predicted levels for test Mach numbers up to 0.9, as shown in Figure A-3. However, at the supersonic cruise Mach number of 2.0, the thrust coefficients were biased approximately 1 percent high, as seen in Figure A-3. It is felt, however, the relative comparisons between supersonic cruise configurations are valid.

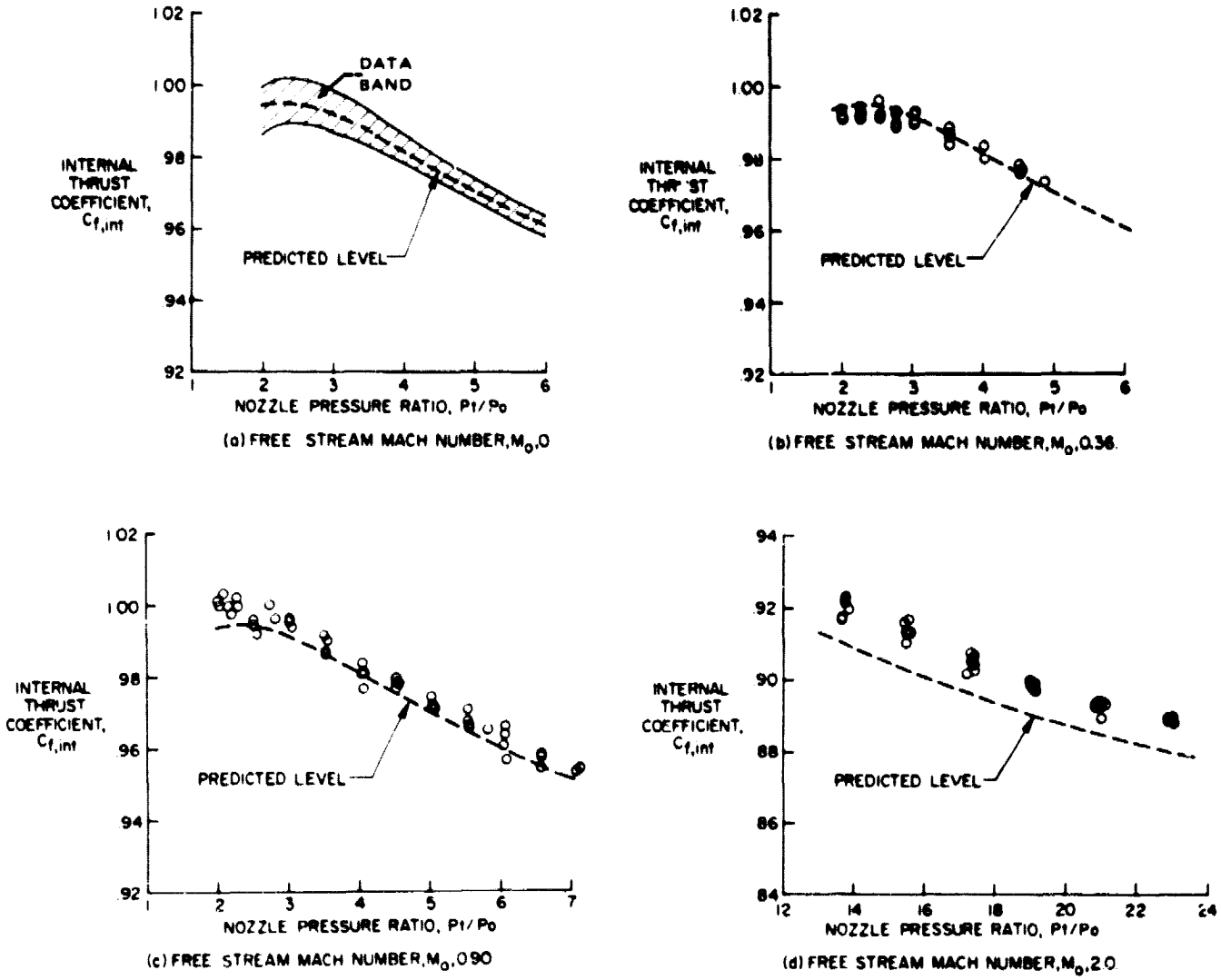

Figure A-3 *Modified Suprsonic Tunnel Association Nozzle Internal Thrust Coefficients.*

APPENDIX B

LIST OF SYMBOLS

		(Equation No.)
A	Area	
B	Base	
C	Constant relating venturi area ratio to one-dimensional pressure ratio	
c	Chord	
C-D	Convergent divergent nozzle	
C_D	Discharge coefficient	(3)
$C_{f\,int}$	Modified Supersonic Tunnel Association nozzle thrust coefficient	(2A)
C_{fp}	Gross thrust coefficient (not including external friction drag)	(18)
D	Diameter, drag	
F	Nozzle generated force, thrust	
g	Gravitational constant	
K	Compressibility correction	
L	Length	
m	Mass flow	
M	Mach no.	
P	Pressure	
R	Gas Constant	
STA	Supersonic Tunnel Association	
T	Temperature	
t	Thickness	
V	Velocity	
W	Weight flow	
$W_{s\ corr}$	Corrected secondary flow	(7)
X	Axial distance	
Y	Radial position	

Greek Letters

α	Ejector inlet flap angle	
β	Trailing edge flap boattail angle	
γ	Specific heat ratio or plug angle	
Δ	Difference of two terms	
δ	Splitter trailing edge included angle	
η	Nozzle efficiency (does not include external friction drag)	(23)
Θ	Shroud internal divergence angle	
τ	Clamshell angle of rotation	
ϕ	Shroud external convergence angle	

APPENDIX B

LIST OF SYMBOLS (Cont'd)

(Equation No.)

Superscripts

*	Sonic flow condition

Subscripts

B	Base
Corr	Corrected
ex	Exit
f	Fan duct
i	Ideal
inlet	Ejector inlet
int	Internal
l	Local
LC	Load cell
Max	Maximum
o	Ambient condition
p	Primary duct
s	Secondary or Shroud
sm	Friction drag on metric portion of model
t	Total
v	Venturi

Numerals

0	Free stream or ambient condition
8	Primary nozzle throat station
8'	Primary nozzle exit station - plug retracted
9	Ejector exit station
18	Fan duct nozzle throat station